

Temperature Response Of Emissivity In Intrinsic Silicon:  
A Selective Absorber For Solar Energy Harvesting

By

CRISTIAN ALONSO HEREDIA

B.S. (Cal-Poly, San Luis Obispo) 2004

M.S. (San Francisco State University, San Francisco) 2008

DISSERTATION

Submitted in partial satisfaction of the requirements for the degree of

DOCTOR OF PHILOSOPHY

in

ELECTRICAL ENGINEERING

in the

OFFICE OF GRADUATE STUDIES

of the

UNIVERSITY OF CALIFORNIA

DAVIS

Approved:

---

Jerry Woodall, Chair

---

Diego Yankelevich

---

Bryan Jenkins

Committee in Charge

2016

Copyright © 2016 by  
CRISTIAN ALONSO HEREDIA  
*All rights reserved.*

*Dedicated to Juana Alonso . . .*

*cruzamos fronteras.*

## CONTENTS

List of Figures . . . . .	v
List of Tables . . . . .	vii
Abstract . . . . .	viii
Acknowledgments . . . . .	ix
<b>1 Introduction</b>	<b>1</b>
<b>2 Background</b>	<b>5</b>
2.1 Photovoltaic Review . . . . .	6
2.2 Concentrated Solar Power Review . . . . .	11
2.3 Emissivity . . . . .	14
2.3.1 Blackbody Radiation . . . . .	15
2.3.2 Spectral versus Hemispherical Emissivity . . . . .	18
2.3.3 Selective Absorbers . . . . .	19
2.3.4 Silicon as a Selective Absorber . . . . .	23
2.4 Solar Conversion Efficiency . . . . .	29
2.5 Levelized Cost Of Electricity . . . . .	31
<b>3 Materials and Methods</b>	<b>35</b>
3.1 Materials . . . . .	35
3.2 Sample Preparation . . . . .	36
3.3 Measurement Protocol . . . . .	37
3.4 Solving for Emissivity . . . . .	37
3.4.1 Solving For Emissivity Relative To A Blackbody . . . . .	39
3.4.2 Solving For Emissivity In The Thermal Decay Region . . . . .	41
<b>4 Results</b>	<b>42</b>
4.1 Solving For Emissivity . . . . .	42
4.1.1 Graphite . . . . .	42

4.1.2	Intrinsic Silicon . . . . .	43
<b>5</b>	<b>Discussion</b>	<b>46</b>
5.0.1	LCOE Revisited . . . . .	47
<b>6</b>	<b>Future Work</b>	<b>49</b>
6.0.1	Optimizing Thickness . . . . .	49
6.0.2	Decreasing Effective Emissivity . . . . .	49
6.0.3	Finding Semiconductors Candidates . . . . .	50
<b>A</b>	<b>Planck's Law Derived</b>	<b>52</b>
A.0.1	Stefan-Boltzmann Law Derived . . . . .	55
<b>B</b>	<b>Theoretical Solar Efficiency Limit</b>	<b>57</b>
<b>C</b>	<b>Supplemental Material</b>	<b>59</b>
<b>D</b>	<b>Copyright Permissions</b>	<b>62</b>

## LIST OF FIGURES

1.1 U.S. Exergy . . . . .	3
1.2 Photothermal Generator . . . . .	4
2.1 Best Research-Cell Efficiencies . . . . .	7
2.2 AM1.5 Spectrum . . . . .	8
2.3 Photovoltaic Schematic . . . . .	9
2.4 Ideal Efficiency Versus Energy Gap . . . . .	11
2.5 Power Tower . . . . .	12
2.6 Parabolic Trough . . . . .	12
2.7 Global CSP . . . . .	13
2.8 Planck's Law Spectral Irradiance . . . . .	16
2.9 Thermal Radiation Wavelengths . . . . .	17
2.10 Visible Spectrum . . . . .	17
2.11 Solid Angle Diagram . . . . .	19
2.12 Steady-state Temperature . . . . .	20
2.13 Ideal Selective Absorber . . . . .	21
2.14 Dendritic and Hillock Tungsten Surfaces . . . . .	22
2.15 Relative Abundance of Silicon . . . . .	24
2.16 Solar Spectrum and Silicon Bandgap . . . . .	25
2.17 Sato's Experimental Schematic . . . . .	26
2.18 Timans' Total Hemispherical Emissivity . . . . .	27
2.19 Silicon Electroluminescence Spectra For Various Silicon Diodes . . . . .	28
2.20 Silicon Electroluminescence Efficiency . . . . .	28
2.21 Silicon Carbide Emission Spectrum . . . . .	29
2.22 Blackbody Relative Intensity . . . . .	29
2.23 Blackbody and Carnot Efficiency . . . . .	31
2.24 Moderate Concentration Efficiency . . . . .	31
2.25 Duck Curve . . . . .	34

3.1	Epoxied Graphite . . . . .	38
3.2	Focused Beam . . . . .	38
3.3	Experimental Schematic . . . . .	39
3.4	Absorber Temperature Response . . . . .	40
4.1	Graphite Heat Capacity . . . . .	43
4.2	Graphite Emissivity Data . . . . .	43
4.3	Intrinsic Silicon Heat Capacity . . . . .	44
4.4	Intrinsic Silicon Emissivity Data . . . . .	44
4.5	Intrinsic Silicon Emissivity Temperature Dependence . . . . .	45
6.1	Intrinsic Silicon Transmittance . . . . .	50
B.1	Heat Diagram . . . . .	57
C.1	Carrier Concentration . . . . .	60
C.2	Custom Flange Schematic . . . . .	60
C.3	Focused Beam Through Lens . . . . .	61

## LIST OF TABLES

1.1	Average annual cooling degree days . . . . .	2
2.1	Photovoltaic efficiencies by technology . . . . .	10
2.2	CSP capacity . . . . .	13
2.3	Dispatchable LCOE . . . . .	33
2.4	Non-Dispatchable LCOE . . . . .	33
3.1	Wafer resistivity . . . . .	37
5.1	Estimated photothermal generation LCOE . . . . .	48
5.2	Power per square foot comparison . . . . .	48
6.1	Semiconductor band gap energy . . . . .	51
C.1	Specifications of components . . . . .	59

## ABSTRACT

### Temperature Response Of Emissivity In Intrinsic Silicon: A Selective Absorber For Solar Energy Harvesting

The National Academy of Engineers named affordable solar energy as one of the grand challenges for the twenty-first century. Even in sunniest U.S. locations, without subsidies, home generation is still cost prohibitive. To address the cost of solar energy, we investigated intrinsic silicon as a low emissivity selective absorber.

We wanted to determine the emissivity of intrinsic silicon at elevated temperatures. At elevated temperatures, a selective absorber coupled to a heat engine could efficiently generate electrical power. Photothermal efficiency depends on the absorber's emissivity. I analyzed total hemispherical emissivity for graphite and intrinsic silicon using a thermal decay method inside a thermal isolation chamber.

The results show low emissivity values for intrinsic silicon. Consequently, for temperatures less than 300 °C, intrinsic silicon has a small emissivity (0.16). This small value is in agreement with doped silicon experiments. However, unlike doped silicon, at elevated temperatures of 600 °C, intrinsic silicon emissivity values remain low (0.33).

Our analysis suggests intrinsic silicon could convert more solar power into heat than an ideal blackbody. Specifically, the harvested heat could drive a heat engine for efficient power generation. Thus, a cost-effective electrical generating system can operate with a small land footprint using earth abundant silicon.

## ACKNOWLEDGMENTS

This was the first page I wrote. There are many people I'd like to thank, without them I don't know if I finish this dissertation.

To my Mentors: Mrs. Villanueva, you were the first person to recognize, acknowledge, and feed the spark in me. Dr. Thomas Bensky, without your graduate school seed planting, I would have overlooked graduate programs. To Dr. Barbara Neuhauser, you re-energized my love for science and made it accessible again. Dr. Susan Lee, you kicked my butt; and, in doing so, reaffirmed the adage "what doesn't kill you, makes you stronger." Hector Cuevas, without your commitment to student retention I would have never survived academia.

I would like to thank the UC Davis Chicana/o Studies Department for adopting me in so many ways. You were my home away from home—allowing me to contribute to my *communidad*. In the sciences, my commitment to my *communidad* was scrutinized. However, after working with Chicana/o studies, I learned my praxis was one of dual-strivings: to my science and to my familia; to my career and to my people—all of them. In attempting to do so, I probably failed. This plight was as violent as a street fight, sometimes with the same rules. Latinos are the largest ethnic group in California. Yet, out of 7000 graduate students at UC Davis, 5% are Mexican-Americans/Chicanos. As the only minority in my Engineering cohort, it's doubtful I graduate without Chicana/o studies support.

My path was unconventional. Directly contributing to my community was paramount to fully realizing my self-determination—Chicano! Mentoring people of color reminded me of the invisible struggle ever present. We are after all, only, human—the shame and the beauty.

To my friends: Thank you, Alonzo Campos, for sharing new methods of getting things done. Liz Cruz, thank you for your encouragement and introducing me to Chicana/o studies. Celina Rodriguez, thank you for humanizing me. Elizabeth (Xamo) Gonzalez, thank you for being my spiritual sister. Denise Gonzalez, thank you for being my buddy. Elenor Castillo, you serve as an inspiration and a sister. Elenor, we suffered and championed

together. Alvaro Marcelo, thank you for being my brother and never leaving my side.

Kyle Westbrook (ECE Graduate Program Coordinator) and Renee Kuehnau (Student Services), thank you for smoothing out the wrinkles.

And to my mother, Maria Torres, and my sister, Liz-Natalie, gracias por todo el apoyo.

Maria: Me enseñaste que el mejor curso de educación es tener fe en la imaginación y los sueños del estudiante. Con amor, Gracias.

-Xristian Heredia

# Chapter 1

## Introduction

We are like tenant farmers chopping down the fence around our house for fuel when we should be using Nature's inexhaustible sources of energy—sun, wind and tide. I'd put my money on the sun and solar energy. What a source of power! I hope we don't have to wait until oil and coal run out before we tackle that.

---

*Thomas A. Edison*

By the time this dissertation is published the price of solar power would have changed, most likely for the better. However, the economic metrics and heat balance equations presented here will still hold true.

The largest and fastest growing cities in the world all experience an energy deficit [1]. Many of these locations—Bangkok, Mumbai, Jakarta, etc.—all have a large number of cooling days and suffer from a lack of established electrical grid (Table 1.1). In many of these locations, grid infrastructure is essentially absent and large-scale residential power is needed. An alternative to large-scale residential power could be a cost-effective photothermal generation technology. Such a technology would help developing economies leapfrog a fossil-fuel infrastructure.

Table 1.1. Average annual cooling degree days in decreasing order. Cooling degree days is an index of the energy demand to cool buildings, calculated by summing up the annual difference of average daily temperature from 65 °F [1].

City	Country	Population [Millions]	Cooling Degree Days
Madras	India	6.9	3954
Bangkok	Thailand	6.6	3884
HoChiMinh	Vietnam	5.1	3745
Ahmadabad	India	5.1	3514
Manila	Philippines	10.7	3438
Jakadrtta	Indonesia	13.2	3390
Mumbai	India	18.2	3386

In the U.S., fossil-fuel combustion still accounts for 82% of U.S. energy sources (Fig. 1.1). However, from 2012 to 2014 U.S. solar generation of retail electricity nearly doubled. Today, photovoltaic generation accounts for most the commercial renewable electricity generated from solar power. Alas, this solar power comes with a low system efficiency of 20%.

Because of low solar conversion efficiencies and a rising global electricity demand we investigated using an earth abundant selective absorber for photothermal conversion. We wanted to determine the emissivity of intrinsic silicon at elevated temperatures. At IBM Woodall et al. studied tungsten emissivity for solar conversion efficiency by using a thermal decay method [2]. Using that method we explored intrinsic silicon as a selective absorber.

This thesis aims to lay the engineering and economic foundation for an efficient photothermal generator. The system generates power by focusing sunlight through an inexpensive plastic Fresnel lens. The lens focuses the light on a highly efficient silicon absorber. The silicon absorber converts solar power to heat. A heat engine takes advantage of the retained heat to generate electricity (Fig. 1.2). In theory, intrinsic silicon as a photothermal conversion can achieve efficiencies as high as 50%.

The payoff is a disruptive generation model for community on-site generated power

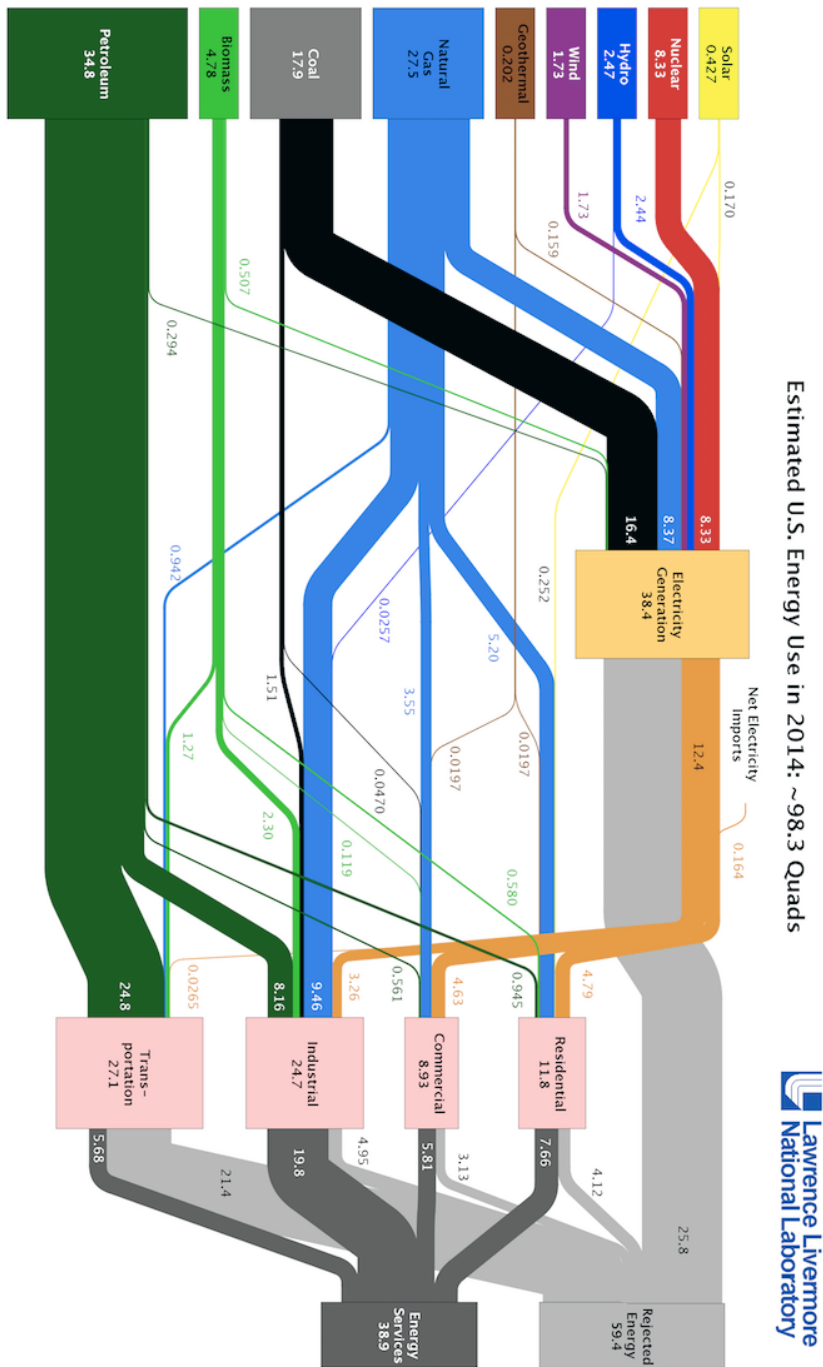


Figure 1.1. Estimated U.S. exergy flow. Source: LLNL 2015. Data is based on DOE/EIA-0035 (2015-3) March 20, 2014

structure. Such a system could be tied into the grid during non-generating hours; or it could charge batteries for an off-the-grid solution.

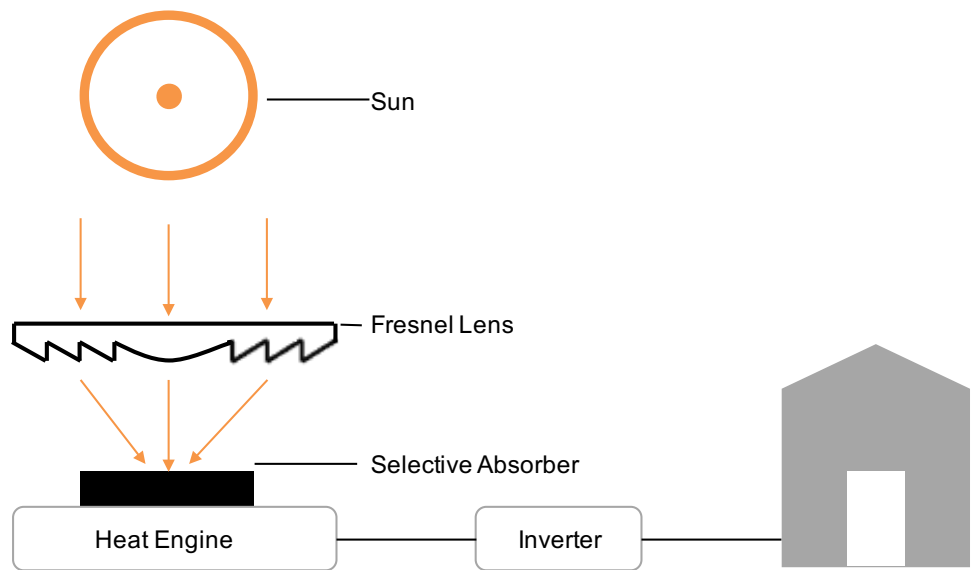


Figure 1.2. Schematic of photothermal generator. Sunlight is focused up to 100x normal concentration ( $1 \text{ kW/cm}^2$ ) onto a selective absorber.

# Chapter 2

## Background

It is not the possession of truth, but  
the success which attends the seeking  
after it, that enriches the seeker and  
brings happiness to him

---

*Max Planck*

This chapter aims to give an overview of the current state of the art for solar generators. It outlines the mechanism of operation and the current state of each technology. Specifically, it outlines two commercially available solar technologies: photovoltaic (PV) generation and concentrated solar power (CSP). The third technology discussed, selective absorbers (SA), is still in the research phase. PV, or solar cells, use the photovoltaic effect. The photoelectric effect excites carriers into available conduction bands. These carriers later get swept out as current. Alternatively, CSP uses high concentrations (100 - 1000x) of solar power to heat a working fluid e.g., water in a tube or a liquefied salt with a high heat capacity. Furthermore, selective absorbers can improve the efficiency of thermal generators. SA do this by capturing more of the Sun's radiation and not re-emitting it as heat. This chapter also outlines the previous selective absorber art. It explains why we chose to investigate intrinsic silicon for heat harvesting. All three technologies, either directly or indirectly, convert light to electricity. Finally, with the levelized cost of energy (LCOE) we describe a figure of merit to calculate the cost of generation.

## 2.1 Photovoltaic Review

In 1954, Bell Telephone developed the first solar cell. In 1958, Vanguard 1 was the first solar powered satellite. These first cells had an efficiency of 6%. Figure 2.1 shows the progress solar cells have made over time. Recently, with government subsidies, PV systems prices have approached grid parity, alternative power prices equivalent to grid prices. PV leveled cost of electricity becomes competitive after reducing installation costs and increasing efficiency. (Typically 50% of a PV system comes from cabling and installation.) Now, as a fully mature technology, utility companies are using efficient PV technology (greater than 20%) for large-area power applications.

Photovoltaic panels offer a direct method to convert photons to electrical power. Sunlight is an assembly of solar energy particles or photons. A photon's energy corresponds to its respective wavelength. Depending on the energy of the photon, and thickness of PV material, it can do one of three things: reflect off the surface, transmit through the cell, or absorb into the material. A photon with energy below the band gap will not absorb, i.e. will fail to excite a carrier into the conduction band. A photon with energy above the band gap will promote a carrier into the conduction band; however, promoted carriers will convert the above band gap energy into heat. Because of these two factors, semiconductors with a band gap of 1.1 to 1.4 eV can convert 45% of the incident solar spectrum. By analyzing solar spectrum photons Shockley and Queisser determined the maximum efficiency for a semiconductor, with a band gap of 1.34 eV under air mass coefficient 1.5 (AM1.5), is 33.7% [3]. (See Fig. 2.2 for AM1.5 spectrum.) Thus, photons with enough energy will excite carriers in the PV material. Due to the material's built-in electric field, depending on charge the excited carriers will get swept out to the substrate surface. Negative (electrons) to one side, positive (holes) the other. Once at opposite sides, the free carriers generate a voltage potential. The voltage potential can power a circuit through a light-generated current (Fig. 2.3). The electrical power is proportional to the radiated power falling on their surface. Therefore, PV panels should directly face the sun. Tracking systems help terrestrial PV systems achieve the most power.

PV technologies are classified into three groupings: first, second, and third-generation.

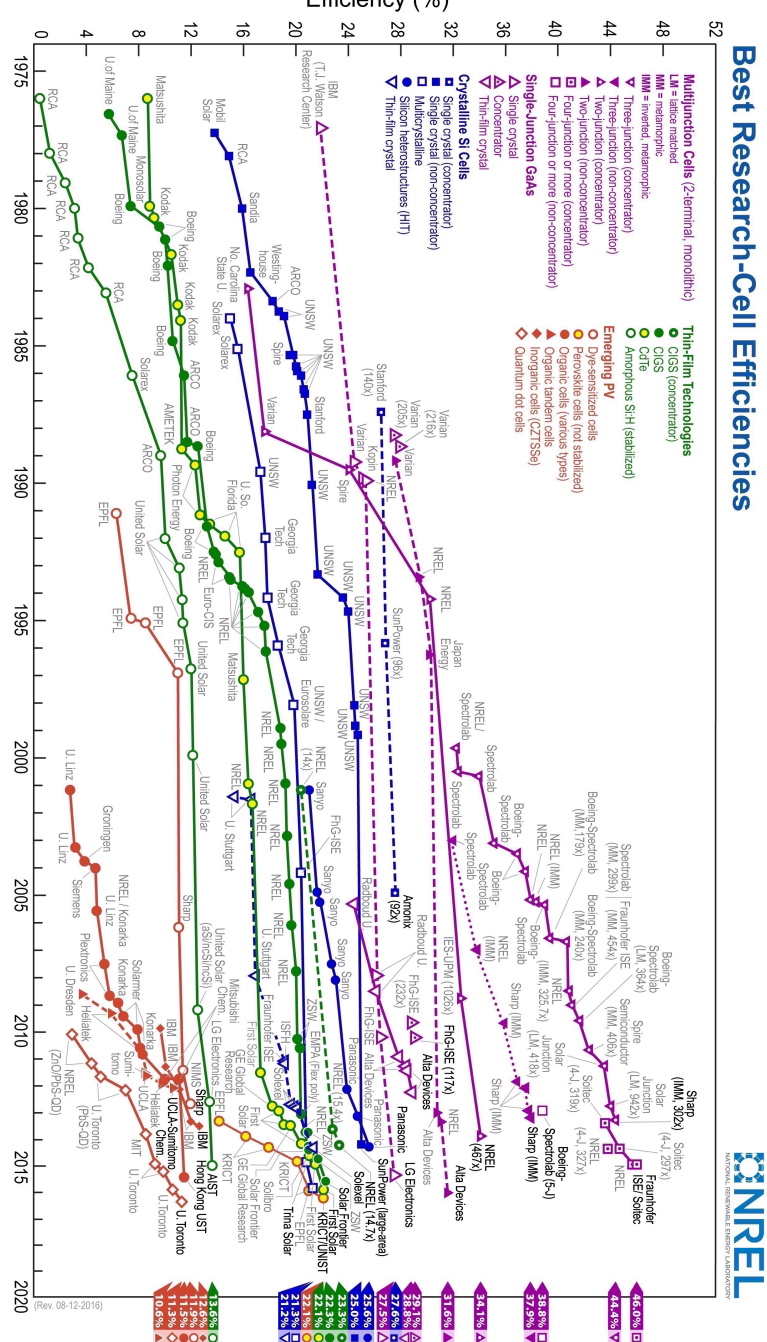


Figure 2.1. Progress of cell efficiency over time. This plot is courtesy of the National Renewable Energy Laboratory, Golden, CO. <http://www.nrel.gov/pv/>

Figure 2.1 shows a progression of all three technologies over time. The most studied first-generation cells are Monocrystalline silicon solar cells. Monocrystalline cells have a planar geometry and they tend to be the most efficient out of the three types. Second-generation

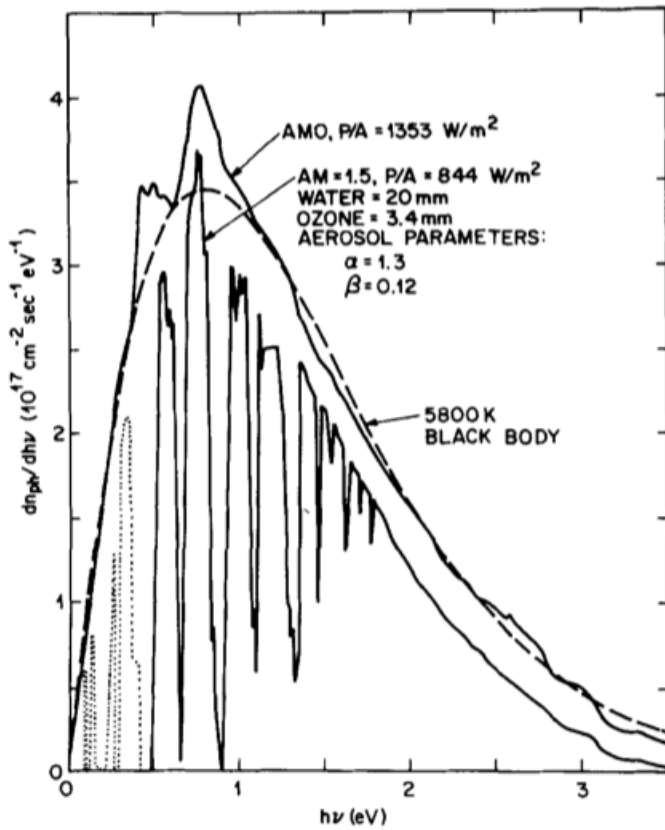


Figure 2.2. Air terrestrial air mass 1.5 spectrum, an extra terrestrial air mass 0 spectrum, and a 5800 K blackbody spectrum [4]. (See Appendix for documentation of permission to republish this material.)

solar cells are constituted by amorphous silicon or non-silicon materials such as cadmium telluride. Second-generation cells are also known as thin-film solar cells. These thin films layers use micrometers of semiconductor layers, instead of whole wafers. The thin layers flex enough to contour to different geometries, such as rooftop shingles or automobile parts. Furthermore, third-generation solar cell research is working towards printable organics and conductive plastics. Third-generation cells are the most inefficient out of the three categories; but, they can be made from inexpensive materials. Regardless of material cost, efficiency is the key driver when it comes to the levelized cost of electricity.

Efficiency for single-junction solar cells has steadily increased over the years. Monocrystalline Si and GaAs are approaching efficiencies of 26 to 29%. Thin-film materials (Si, CIGS, CdTe, perovskite) are in the 20 to 22% range. All other materials show efficiencies in the 10 to 13% range. Figure 2.1 suggests efficiency records will continue to be broken in

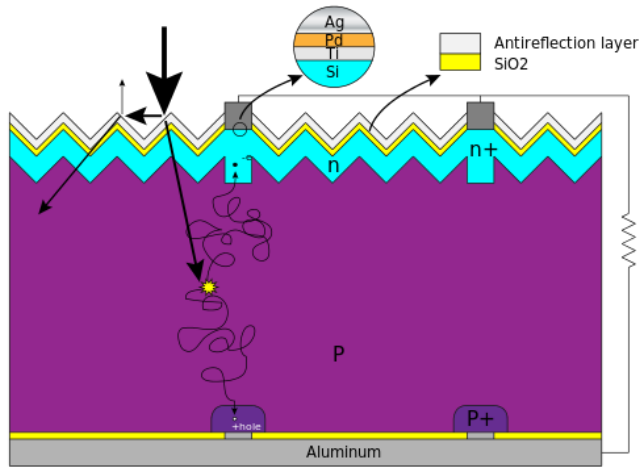


Figure 2.3. Due to a built-in electric field, any excited carriers will get swept out to the substrate surface. Negative (electrons) to one side, positive (holes) the other. Once at opposite sides, the free carriers generate a voltage potential. (Source: Cyferz CC BY 3.0 (<http://creativecommons.org/licenses/by/3.0>), via Wikimedia Commons.)

the future. However, the photovoltaic conversion comes with an upper limit. Figure 2.4 shows the maximum efficiencies of ideal solar cells are calculated for both single energy gap cells using a standard air mass 1.5 terrestrial solar spectrum. At a concentration of 1 sun, the maximum theoretical efficiency is 31%. At a concentration of 1000 suns with the cell at 300 K, the maximum theoretical efficiency is 37% [4]. The Queisser-Shockley limit derives the theoretical limit of single-junction silicon PV at 33.7% [3]. This limit is paramount because single-crystal PV is approaching its theoretical limit. Interestingly, cell efficiency does increase when using multi-junction technology. However, p-n junction emission, light radiated from junctions, leads to energy losses. Additionally, layered cells increase the fabrication complexity and costs.

Efficiency is greatest for matured technologies. Yet, second-generation technologies are making progress (Fig. 2.1). Each technology has an addressable strength (Table 2.1). At the end of this chapter, we see efficiency plays a crucial role in calculating generation cost.

Table 2.1. Photovoltaic efficiencies by technology. Monocrystalline PV dominates the commercial PV market [5].

Mature, large scale	Cell $\eta$ [%]	Module $\eta$ [%]	Notes
Monocrystalline Si	25.6	22.4	Earth abundant material >25 year track record
Multicrystalline Si	21.3	18.5	Earth abundant material >25 year track record
CIGS	21.7	17.5	Flexible structures Solution processing
CdTe	21.5	18.6	Flexible structures
Emerging, small scale			
Dye-sensitized TiO <sub>2</sub>	11.9	10	Tunable band gap Stability issues
Thin film SI	11.4	12.2	Flexible structures
Organic	11.5	9.5	Tunable band gap Stability issues
GaAs	28.8	24.1	High efficiency Intensive processing
Perovskite	21	N.A.	Solution processing Stability issues
Quantum Dots	9.9	N.A.	Solution processing

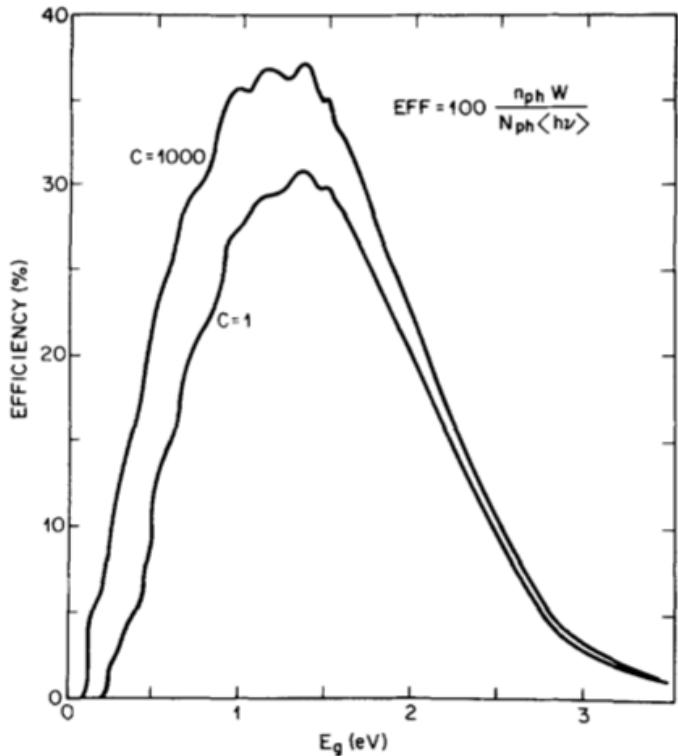


Figure 2.4. Solar Cell efficiency versus energy gap for solar concentrations of 1 and 1000 suns [4]. (See Appendix for documentation of permission to republish this material.)

## 2.2 Concentrated Solar Power Review

Concentrated solar power generates electricity using venerated technologies. A fossil-fuel power plant uses combustion to generate heat. This heat forces water through a steam engine, which converts mechanical to electrical power. In contrast, CSP harvests heat with high concentrations (100 - 1000x) of solar power. Heat is collected in a power tower through an array of heliostats, an array of planar mirrors (Fig. 2.5). Another collection method heats receiver tubes through a series of parabolic trough mirrors (Fig. 2.6). The mirrors concentrate light and heat a working fluid, which in turn drives a turbine. Through concentration, power towers reach temperatures of 500-1000 °C; parabolic troughs, 150-350 °C.

Through exponential growth (Fig. 2.7) in the last decade, CSP is orienting itself to become a primary source of renewable power in the U.S. The National Renewable Energy Laboratory (NREL) provided research and development efforts to advance CSP, from



Figure 2.5. An example of power tower surrounded by heliostats. (Source: By afloresm (SOLUCAR PS10) [CC BY 2.0 (<http://creativecommons.org/licenses/by/2.0>)], via Wikimedia Commons)



Figure 2.6. An example of a parabolic trough. Harper Lake, California. (By Z22 (Own work) [CC BY-SA 3.0 (<http://creativecommons.org/licenses/by-sa/3.0>)], via Wikimedia Commons)

generation to transmission to distribution to the end user. To date, global CSP nameplate capacity installed is 3425 MW. CSP plants are useful for large land footprint locations and large scale power demands. (See Table 2.2 for an example of CSP footprint and power output.) To help put this into perspective, the average U.S. house uses 911 kWh per month. According to Table 2.2, four of the five largest CSP plants reside in California.

Table 2.2. Capacity for the largest CSP generators in the world [6].

Facility	Capacity [MW]	Area [acres]	Location
Ivanpah Solar Power Facility	392	3500	Ivanpah, Ca
Solar Energy Generating System	354	1600	Mohave Desert, Ca
Mojave Solar Project	280	1765	Barstow, Ca
Solana Generation Station	280	1920	Gila Bend, Az
Genesis Solar Energy Project	250	1920	Blythe, Ca

California is rated for 5 hours of peak sun hours. With that much insolation, solar radiation flux, the average CSP can potentially power up to 1372 homes.

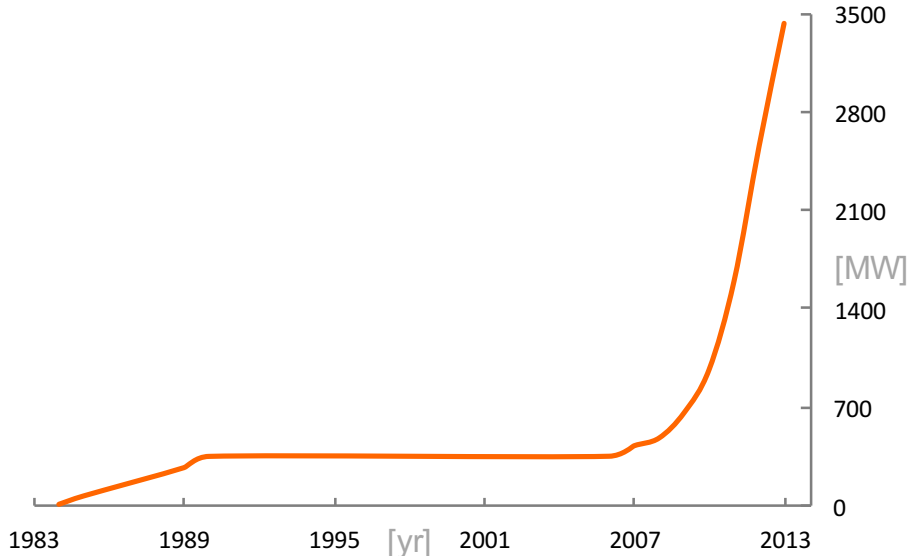


Figure 2.7. Global CSP installation (Mega Watts) reached exponential growth in 2007 [6].

CSP plant improvements will come from economies of scale, cost reductions, and conversion efficiency. When it comes to Carnot efficiency, the higher the operating temperature the better. Higher operating temperatures can be achieved by using molten salts for heat transfer and storage. Compared to PV, CSP plants benefit from high differential temperatures and potential storage. If they continue to improve, they will gain market penetration wherever capital is available.

CSP are capital intensive. Because of this initial cost, the LCOE for CSP plants is currently high, 239.7 \$/MWh. (See Tables in Levelized Cost Of Electricity for renewable energies comparison.) Adding thermal storage capabilities increases the initial plant investment costs. But the storage potentially doubles the capacity factor, the ratio of real output to full capacity.

PV and CSP each have their advantages and disadvantages. The portability of PV is convenient for small applications. However, the large scale of CSP is convenient for storing thermal energy; CSP energy storage makes it dispatchable, capable of matching a markets demand profile. Once an economical storage solution becomes available, PV will dominate the energy market. Until then, CSP is becoming a commercially viable solution.

## 2.3 Emissivity

The second law of thermodynamics requires that energy flow is always toward a more uniform distribution of energy in the universe. Incidentally, everything in the universe glows with radiation from its own internal heat. Heat is the energy of an object's internal particles. Heat transfers using a combination of the following three methods: conduction, convection, or radiation. For objects isolated in a vacuum, radiation is the only form of heat transfer. The rate of heat transfer depends exclusively on the value of emissivity.

The rate of energy transfer for a heated object with respect to an ideal blackbody, at the same temperature, is the emissivity of an object. (Emissivity refers to a material's property, while emittance refers to specific samples or objects.) By definition, emissivity is a dimensionless value. The mathematical expression for emissivity is given by

$$\varepsilon = \frac{q_e}{q_B} \quad (2.1)$$

where  $q_e$  is the total hemispherical emissive flux of an object, and  $q_B$  is total hemispherical blackbody flux.

Prior emissivity research used optical measurements, such as reflectance and transmittance readings to calculate emissivity [7, 8]. However, such methods do not directly

measure hemispherical emissivity. Additionally, these optical methods introduce an estimated relative experimental error of 20-30% [9].

This section discusses blackbody emission properties, spectral emissivity, and total hemispherical emissivity. Understanding these three topics allows us to calculate an object's emissivity from temperature. Additionally, understanding the physics of emissivity will help define an ideal selective absorber.

### 2.3.1 Blackbody Radiation

An ideal blackbody absorbs and emits all wavelengths equally. Planck describes the origins of emission from a material as:

The creation of a heat ray is generally denoted by the word emission. According to the principle of the conservation of energy, emission always takes place at the expense of other forms of energy (heat, chemical or electric energy, etc.) and hence it follows that only material particles, not geometrical volumes or surfaces, can emit heat rays. It is true that for the sake of brevity we frequently speak of the surface of a body as radiating heat to the surroundings, but this form of expression does not imply that the surface actually emits heat rays. Strictly speaking, the surface of a body never emits rays, but rather it allows part of the rays coming from the interior to pass through. The other part is reflected inward and according as the fraction transmitted is larger or smaller the surface seems to emit more or less intense radiations. (Planck, 1914) (See Appendix for documentation that this material is in the public domain.)

Above Planck states that radiation may not originate at the surface, but indeed the surface alters the emissivity of an object.

Kirchoff's radiation law states that for any radiating or absorbing body (e.g. solar-absorbing materials), absorptance equals emissivity at a given wavelength. Kirchoff's radiation law is a consequence of conservation of energy; otherwise, a blackbody would be hotter or colder than its environment—not physically possible. A blackbody reaches thermal equilibrium with the environment by radiating away or absorbing energy. An

ideal blackbody perfectly absorbs all wavelengths, that is absorptivity equals unity. Absorptance gives a material's surface effectiveness of absorbing radiant energy; it measures the fraction of the incident power that absorbs at an interface. Absorptance should not be confused with the absorption coefficient, which measures the ratio of the absorbed to the incident electric field. To summarize Kirchhoff's radiation law: Good absorbers make good emitters.

Rayleigh-Jeans laid down the fundamental derivation for heated body radiation:  $8\pi k_B T / \lambda^4$ . But, that expression becomes problematic at small wavelengths, see Fig. 2.8, a concept known as the ultraviolet catastrophe. To overcome the UV catastrophe, Planck added the Bose-Einstein distribution—the second term in Eq. 2.2. The Bose-Einstein distribution gives the probability of photon energy emitted with respect to wavelength and temperature. At the Sun's temperature, a blackbody would have spectral intensity shown in Figure 2.8. The Blackbody spectral intensity,  $I_{B,\lambda}$ , is given by Planck's Law,

$$I_{B,\lambda} = \frac{2hc^2}{\lambda^5 \left( e^{\frac{hc}{\lambda kT}} - 1 \right)} \left[ \frac{W}{m^2 sr \mu m} \right] \quad (2.2)$$

where  $c = 3 \times 10^8 \text{ m/s}$ ,  $h = 6.626 \times 10^{-34} \text{ Js}$ ,  $k_B = 1.3806 \times 10^{-23} \text{ J/K}$ .

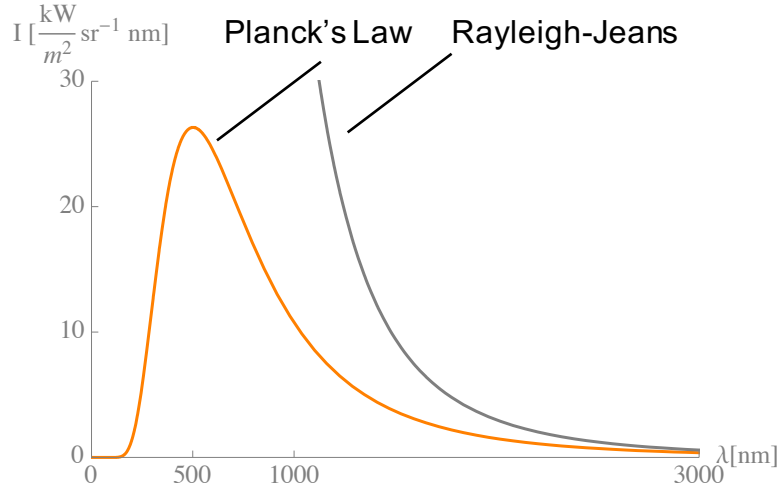


Figure 2.8. Irradiance as a function of wavelength. Planck's Law juxtaposed Rayleigh-Jeans demonstrates the ultraviolet catastrophe at smaller wavelengths. The orange line represents a blackbody spectrum at the Sun's temperature,  $T = 5778 \text{ K}$ , with peak emission near  $\lambda = 500 \text{ nm}$ .

For solar radiation, equivalent to the blackbody temperature of 5778K, the blackbody

spectrum peaks in the green part of the visible spectrum,  $\lambda = 500\text{nm}$ . (This might explain why human vision evolved to have the greatest sensitivity at green wavelengths, Fig. 2.10.) The spectrum's peak wavelength can be found by differentiating Planck's law, with respect to wavelength. This is known as Wien's displacement law:

$$\frac{dI_{B,\lambda}}{d(\lambda)} = 0 \quad (2.3)$$

$$\lambda_{\max}T = 2899.78\mu\text{mK}$$

Blackbody emission or thermal radiation depends only on temperature. Thermal radiation according to Planck's law in theory extends all of the visible spectra. Yet it only covers a small segment of the electromagnetic spectrum. Figure 2.9 visualizes the spectrum coverage.

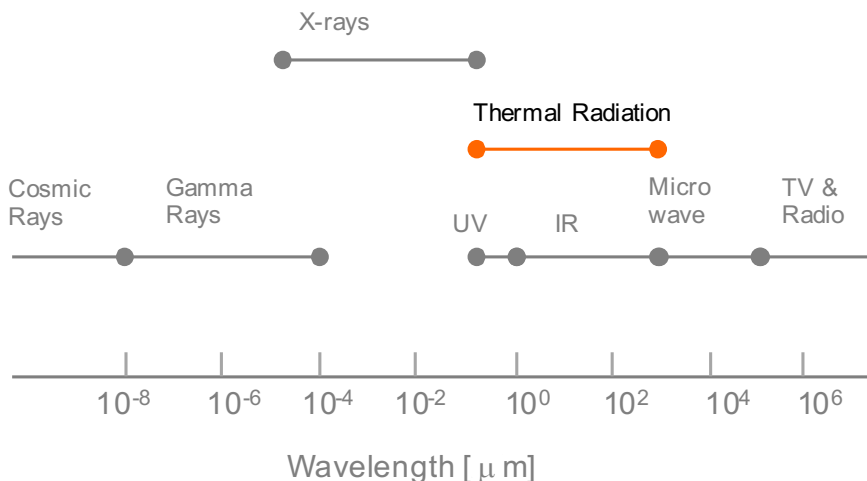


Figure 2.9. Thermal Radiation (emission depends on temperature) extends from  $0.1$  to  $1000\ \mu\text{m}$  in the electromagnetic-wave spectrum. In this figure, the visible spectrum is not visible; it extends from  $0.4$  to  $0.7\ \mu\text{m}$ .

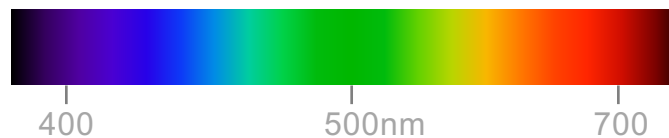


Figure 2.10. Visible spectrum centered about solar blackbody spectrum peak,  $500\text{nm}$ .

## 2.3.2 Spectral versus Hemispherical Emissivity

### 2.3.2.1 Spectral Emissivity

Planck's law specifies radiative power through a solid angle interval. This interval subtends an area element perpendicular to the direction of radiation. Integrating over a hemisphere gives the spectral hemispherical blackbody flux,  $q_{B,\lambda}$ :

$$\begin{aligned} q_{B,\lambda} &= \int_0^{2\pi} \int_0^{\pi/2} I_{B,\lambda} \cos \theta \sin \theta d\theta d\phi \\ &= I_{B,\lambda} \int_0^{2\pi} \int_0^{\pi/2} \cos \theta \sin \theta d\theta d\phi \\ &= \pi I_{B,\lambda} \left[ \frac{W}{m^2 \mu m} \right] \end{aligned} \quad (2.4)$$

This emissive flux is dependent on wavelength and temperature.

### 2.3.2.2 Hemispherical Emissivity

Since  $I_{B,\lambda}$  radiates isotropically, we easily integrate with respect to azimuthal and polar angles. In addition, to obtain the total hemispherical blackbody flux, we integrate over all wavelengths, where  $q_e$  = total hemispherical emissive flux and  $q_B$  = total hemispherical blackbody flux,

$$\begin{aligned} q_B &= \pi \int_0^\infty q_B(T) d\lambda \\ &= \left( \frac{2\pi^5 k^4}{15c^3 h^3} \right) T^4 \\ &= \sigma T^4 [W/m^2] \end{aligned} \quad (2.5)$$

The term in parenthesis is the Stefan-Boltzmann constant,  $\sigma = 5.67 \times 10^{-8} Js^{-1} m^{-2} K^{-4}$ . The above equation depicts the Stefan-Boltzmann law and gives the total blackbody radiative power over all angles and all wavelengths, displayed in Fig. 2.11.

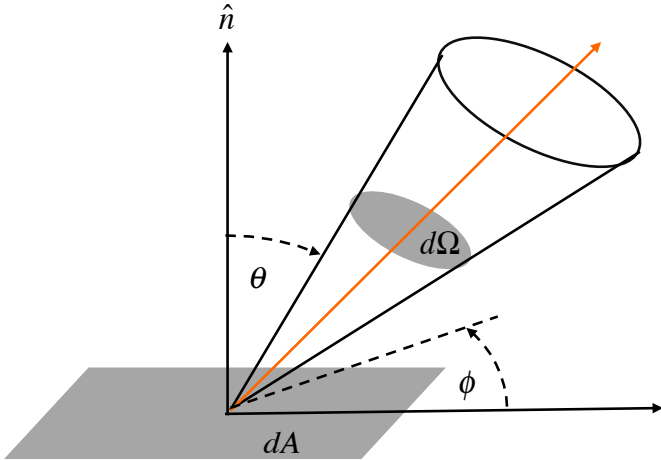


Figure 2.11. Defining solid angle for emitted radiation from a point source.

Now we have a mathematical expressions for the emissivity definition given in Eq. 2.1, which can be written as the Stefan-Boltzmann relationship, derived in Appendix A.0.1.

$$P = A\varepsilon\sigma(T^4 - T_0^4)[W] \quad (2.6)$$

where  $P$  is the power,  $A$  is the radiating area,  $\varepsilon$  is the emissivity,  $\sigma$  the Stefan-Boltzmann constant,  $T$  is the substrate temperature, and  $T_0$  is the ambient temperature.

According to Stefan-Boltzmann law as emissivity decreases, steady-state temperature increases. Figure 2.12 demonstrates this point. This means that a low emissivity material will have a hotter operating temperature than a blackbody, given the same input power. This hotter operating temperature results in improved Carnot efficiency. Because Carnot efficiency increases, the system efficiency (a product of two efficiencies) will also increase.

### 2.3.3 Selective Absorbers

Blackbodies, unlike selective absorbers, absorb over all wavelengths. And, thus, will re-radiate over all wavelength ranges too. In contrast, by not re-radiating everywhere, selective absorbers convert solar power into heat. The solar conversion efficiency of a selective absorber depends on its optical properties. An ideal selective absorber converter absorbs over the entire solar spectrum while minimizing re-radiative losses at longer wavelengths. A good selective absorber for photothermal energy conversion possesses the following properties:

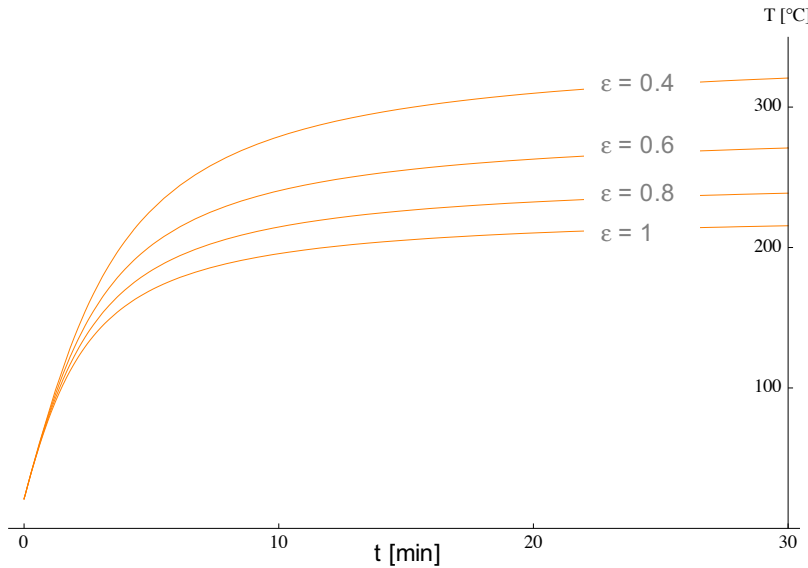


Figure 2.12. Decreasing the emissivity of a selective absorber increases its steady-state temperature according to Eq. 2.6. This simulation assumes an incoming power flux of  $4W/cm^2$  and surface area of  $1cm^2$ .

- Spectral selectivity
- Thermal conductivity
- Thermal stability

The spectral selectivity of an ideal selective absorber behaves like a step function (Fig. 2.14). It absorbs wavelengths up to a critical wavelength. This binary mechanism is not achievable in practice. However, a semiconductor that can absorb up to a certain photon energy will behave similarly. Good thermal conductivity is desired for transferring energy to a heat engine. Thermal stability is needed because the absorber will receive continuous solar concentration. The following sections outline realized semiconductor selective absorbers and their limitations.

#### 2.3.3.1 IBM Research: A new concept for solar energy thermal conversion

In the 1970's, IBM (Woodall, DiStefano, Pettit, and Cuomo) explored materials with low emissivity by utilizing light trapping in a "geometric maze" like medium. They wanted to find materials with good visible spectrum absorptivity and low emissivity. Instead of using good solar absorption materials, they proposed a dense needle-like surface.

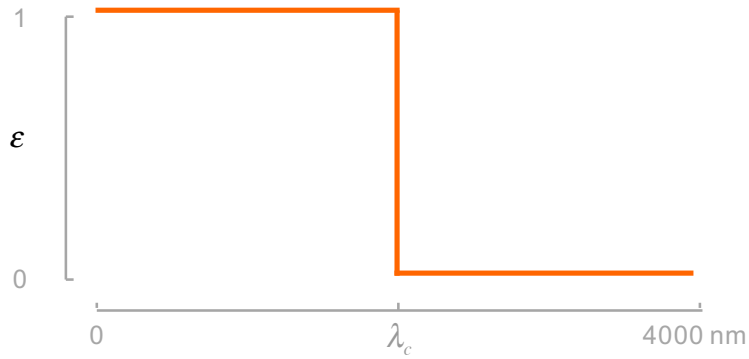


Figure 2.13. Spectral response for an ideal selective absorber.

The diameters of the needles were on the order of visible wavelengths. Since geometry dominates absorption, they proposed a light trapping material. This material also needed to emit poorly in the infrared wavelengths. All of these characteristics needed to happen at power plant temperatures. The highly absorbing surfaces made with low-emitting materials yielded efficient solar thermal converters.

Tungsten single-crystal whiskers, or dendrites, were grown on various substrates—sapphire, tungsten, and stainless steel. Dendrites were grown by hydrogen reduction of tungsten hexafluoride ( $\text{WF}_6$ ). Tungsten's excellent absorption properties, 98%, over a broad spectrum, 0.4-40  $\mu\text{m}$ , with an emissivity of 0.28 make it an excellent candidate for solar absorption. After depositing thin tungsten films,  $\ll 25 \mu\text{m}$ , the surface appeared to be hillock with angles greater than 90°. For thicker films,  $\gg 25 \mu\text{m}$ , dendritic cone structures were formed with angles less than 90°. The dendritic films appeared black due to multiple reflections of incident light (Fig. 2.14).

Woodall et al. used two methods to solve for emissivity:

1. In the first method, due to the samples being placed in a medium vacuum, the heat transfer resulting from conductive and convective cooling can be neglected. Hence the cooling process was purely radiative. Emissivity was measured by thermal decay, where a drop in temperature occurs over a time interval, with the following heat balance equation,

$$P = A\varepsilon\sigma(T^4 - T_0^4) = \frac{dQ}{dt} = \frac{d}{dt}(mc\Delta T) \quad (2.7)$$

where m is the mass and c is the specific heat of the sample.

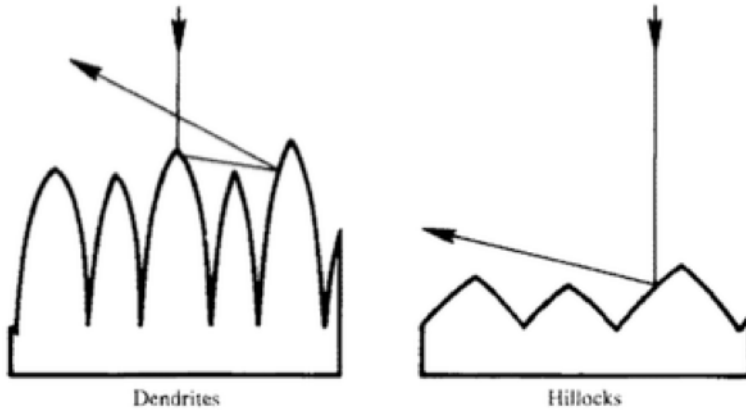


Figure 2.14. Schematic representation of ray scattering on a normally incident light for dendritic and hillock tungsten surfaces. Note: Dendritic structures are  $\ll 25 \mu\text{m}$  and hillock angles are  $>90^\circ$ . For dendritic surfaces, normal incident radiation is forced to undergo two or more reflections before reemission. For the hillock surfaces, the fiber heights are short, resulting in two or fewer bounces before reemission.

Samples were heated in vacuum, then dropped into blackbody cavity. The temperature was read off with fine thermocouple wires. A total emissivity value can be extrapolated by using the following equation,

$$\varepsilon = \frac{C_p(\Delta T/\Delta t)}{A\sigma(T_0^4 - T_S^4)} \quad (2.8)$$

where  $T_S$  = sample temperature,  $C_p$  = heat capacitance,  $A$  = sample area,  $T_0$  = background temperature [2].

2. In contrast, the second method used steady-state temperature conditions to determine the electrical power needed to sustain a given temperature. Then, with knowledge of temperature and incoming power and radiating area size, emissivity can be solved for using the Stefan-Boltzmann law.

Measurements from both methods were in agreement. Both yielded hemispherical emissivity values for dendrites in the 0.26-0.30 range. Anodized anti-reflective coatings, WF<sub>6</sub>, reduced hemispherical emissivity to 0.18 for hillock surfaces. However, dendritic surfaces with anti-reflection coatings had a greater emissivity, 0.5.

Because of the dendrite geometric factor, absorption quickly attenuates; non-normal incident radiation easily escapes due to fewer reflections of the incident light. Anodized black dendritic surfaces exhibited low reflectivity in the visible wavelengths,  $2.5 \times 10^{-4}$ .

In addition, the dendritic tungsten structures needed a film thickness greater than  $25 \mu m$  to reach high absorption. Thick dendrite films, due to high emissivity values (0.55), were not suited for low-temperature solar collectors.

Moreover, temperatures above 523 K permanently changed the optical properties of the antireflection oxide,  $WF_3$ . This change reflectivity resulted in a slow and irreversible reduction in absorption. The change destroyed the surface selective absorption properties.

The work concluded that when dealing with geometric factors, emissivity depends on the incident angle. It also defined an ideal absorber as having total absorptivity over the visible spectrum and zero emissions in the infrared. It defined a method for calculating emissivity with thermal decay and a method for calculating selective absorber solar conversion (Section 2.4).

### 2.3.4 Silicon as a Selective Absorber

Silicon as a selective absorber is a good candidate for the following reasons: According to the U.S. Geological Survey, silicon is the second most abundant element on the surface of the earth (Fig. 2.15); in other words, scarcity of source material is not an issue. Also, since the advent of silicon transistors (the 1950's), silicon manufacturing technologies have fully matured; this makes purchasing bulk silicon fairly common. Furthermore, silicon's moderate band gap (1.12 eV) completely absorbs visible solar radiation (Fig. 2.16).

In 1966, Sato first investigated the emissivity of silicon [7]. He examined n-type lightly ( $15 \Omega cm$ ) and heavily ( $0.007 \Omega cm$ ) doped silicon for spectral emissivity. Using optical methods, he observed emissivity, from 0.4 to  $15 \mu m$ , in the temperature range 340 K to 1070 K [7]. He measured spectral emissivity using the experimental setup in Fig. 2.17. The experiment did so by spectrally comparing the output from a specimen to that of graphite. The graphite served as a blackbody reference; both items were heated in the same chamber.

Sato identified the three types of thermal radiation for silicon:

- Lattice vibrations
- Band-to-band transitions

- Free carrier emission

At low temperatures, where doped silicon is extrinsic, most of the radiation came from lattice vibrations. At temperatures above 570 K silicon becomes intrinsic. At these temperatures, band-to-band transitions dominate emission. Because the band gap is larger than thermal energy, this radiation only occurs at elevated temperatures. In the case of heavily doped silicon, free-carrier radiation was prominent even at low temperatures. Regardless of heating method, these results were consistent.

Like Sato, Timans [8] executed an optical experiment with light ( $78 \Omega cm$ ) and heavily ( $0.012 \Omega cm$ ) doped silicon. Note that Sato and Timans were measuring spectral emissivity, not total hemispherical emissivity. Calculating hemispherical emissivity from spectral involves many steps. For a given temperature, the sample's spectral emissivity is multiplied by a blackbodies spectra. The resulting products are then integrated to find total hemispherical emissivity. This is not a direct measurement of hemispherical emissivity. Figure 2.18 shows Timans' and Sato's individual results.

For amorphous silicon, White et. al [10] argue the mechanism for absorption and emission. They speculate that absorption is due to the high impurity content in the sample and that an increase in absorption at longer wavelengths may be due to a particular

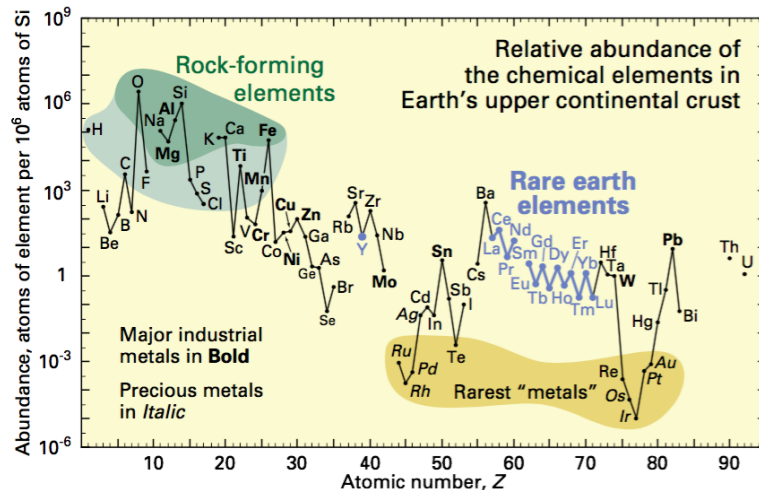


Figure 2.15. U.S.G.S., Compared to rare earth metals, silicon exists in abundance on the surface of the earth (USGS, 2005). (By Gordon B. Haxel, Sara Boore, and Susan Mayfield from USGS; (<http://pubs.usgs.gov/fs/2002/fs087-02/>) [Public domain], via Wikimedia Commons)

distribution of these states. However, they hypothesized that free carriers had little dependence on temperature. This is in disagreement with the previous art. In summary, White concluded that residual absorption observed in these amorphous silicon samples makes them inefficient as selective absorbers for photothermal converters.

The preceding optical emissivity experiments on doped silicon found:

1. The visible spectrum emissivity was high due to band-to-band transitions.
2. The near infrared emissivity was low at low temperatures. The samples were transparent to wavelengths longer than  $1.2 \mu m$ . Hence, the emissivity is low near the infrared. At about 570 K doped silicon becomes intrinsic, and free carrier emission dominates.
3. For wavelengths longer than  $6 \mu m$ , emissivity is high due to lattice vibrations. At about 870 K, due to intrinsic behavior, free carrier emission conceals lattice vibration emissions.

To model spectral emissivity, the three components contributing to emissivity need to be understood,  $\varepsilon(\lambda, T)_{Total} = \varepsilon(\lambda, T)_{Free\ Carrier} + \varepsilon(\lambda, T)_{Absorption\ Edge} + \varepsilon(\lambda, T)_{Phonon}$  [11]. The emissivity components are studied by measuring temperature and spectral emission.

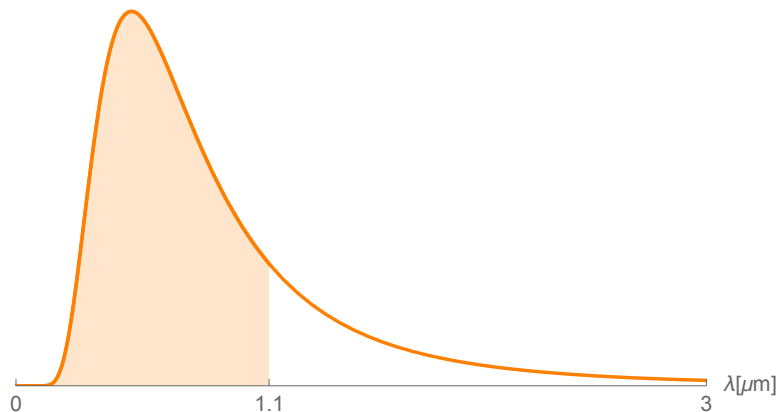


Figure 2.16. The orange line represents the spectral irradiance for a blackbody at the temperature of the Sun. The energy band gap of silicon, 1.12eV corresponding to  $1.1 \mu m$ , is small enough to absorb the visible spectrum. Filled-on region represents photons with energy greater than the absorption edge.

In order to isolate a specific emissivity, the overlapping emissivity must be subtracted. Optical measurements for spectral emissivity can be an error-prone process,  $\pm 10$  °C [11].

Spectral emissivity is useful for processes when specific optical pyrometer data is desired, e.g. Rapid Thermal Processing. Spectral emissivity over the thermal infrared is useful for remotely monitoring energy transfer. Knowledge of spectral emissivity can help build a thermal signature for specimens. Total emissivity can be measured from spectral emissivity,

$$\varepsilon = \frac{\int_0^{\infty} \varepsilon_{\lambda} q_{B,\lambda}(T) d\lambda}{\int_0^{\infty} q_{B,\lambda}(T) d\lambda}. \quad (2.9)$$

However, the most direct method to measure total hemispherical emissivity is with the Stefan-Boltzmann law, Eq. 2.6.

#### 2.3.4.1 Semiconductor Luminescence

When photons with energy above the band gap are absorbed, the excited carriers convert the extra energy into kinetic energy,  $E_{K.E.} = E_{photon} - E_g$ . The photogenerated carriers transfer excess energy to the lattice through thermalization, the process of repeated collisions with the lattice; this cooling process happens on the order of the picoseconds.

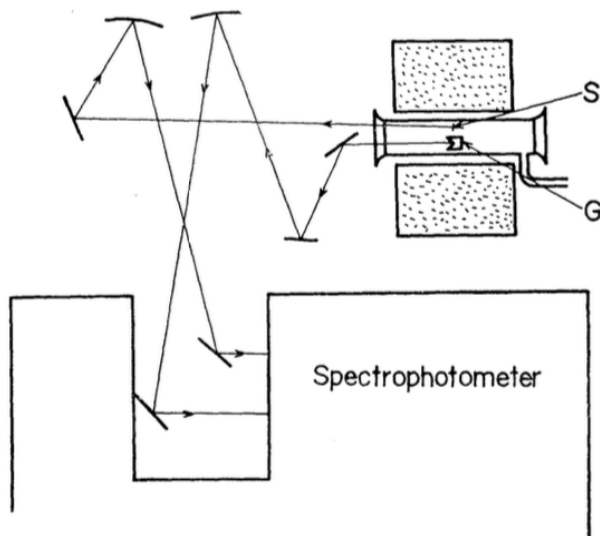


Figure 2.17. Schematic for Sato's optical measurement arrangement with graphite (G) and specimen (S). The samples were placed at the center of an electric furnace [7]. Copyright 1967 The Japan Society of Applied Physics. (See Appendix for documentation of permission to republish this material.)

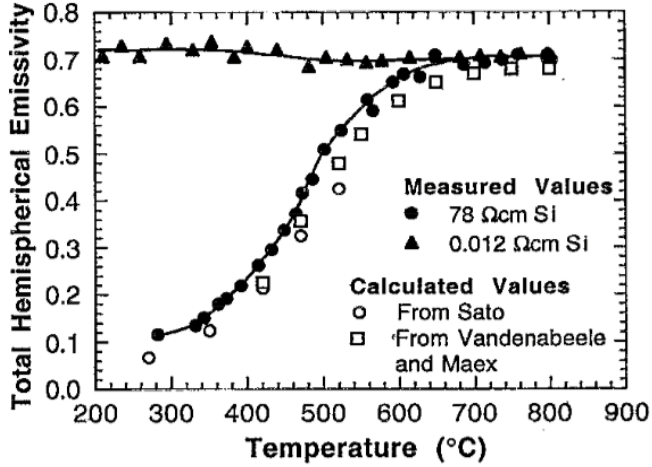


Figure 2.18. Emissivity of lightly ( $78 \Omega\text{cm}$ ) and heavily ( $0.012 \Omega\text{cm}$ ) doped silicon as a function of temperature [8]. The solid curves are fits to the data points. (See Appendix for documentation of permission to republish this material.)

Eventually, the photogenerated carrier will recombine using one of the following methods: Auger, non-radiative via trap state, and radiative band-to-band recombination.

For radiative non-blackbody emitters, Wurfel demonstrates Planck's law for thermal radiation, accounting for chemical potential, extends to radiation of any kind [12]. For a direct bandgap semiconductor, GaAs light emitting diode band-to-band luminescence was calculated and detected by Wurfel [12]. For an indirect bandgap semiconductor, silicon luminescence was measured by Green [13]. Green records low emissions for silicon (Fig. 2.19). Silicon's light-emitting power conversions were on the order of 1% for band-to-band recombination (Fig. 2.20). The silicon results demonstrate that much of the light emitted during radiative recombination is re-absorbed or reflected internally with only a fraction reaching the exterior.

For a direct band gap semiconductor, free of parasitic recombination sites, a photo-generated carrier will eventually radiatively recombine. However, due to the inefficient light-emitting properties of silicon, a carrier will thermalize and contribute to lattice heating. According to Wein's displacement law (Eq. 2.3) heating an object to  $600^\circ\text{C}$  will center the thermal spectral emission peak at  $3.3 \mu\text{m}$ . Figure 2.22 shows that at  $3.3 \mu\text{m}$  intrinsic silicon, without the presence of free carrier absorption, does not have a strong mechanism for emission: The band gap absorption edge is at  $1.1 \mu\text{m}$ , and the lattice

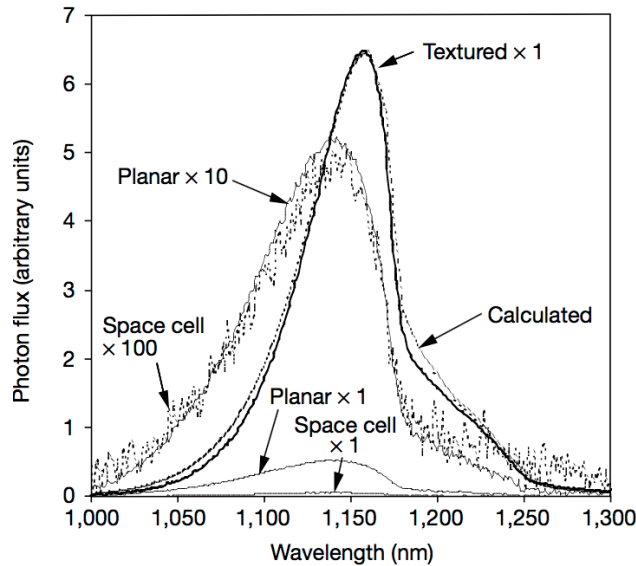


Figure 2.19. Spectra for textured, planar and baseline high efficiency solar cell diodes under 130 mA bias current at 298 K (diode area  $4 \text{ cm}^2$ ) [13]. The 1,10, and 100x denote signal amplification. (See Appendix for documentation of permission to republish this material.)

vibration absorption edge begins at  $6 \mu\text{m}$ . In the patent *Incandescent light energy conversion with reduced infrared emission*, Woodall exploits this selective radiative property to reduce infrared emission with silicon carbide [14] (Fig. 2.21).

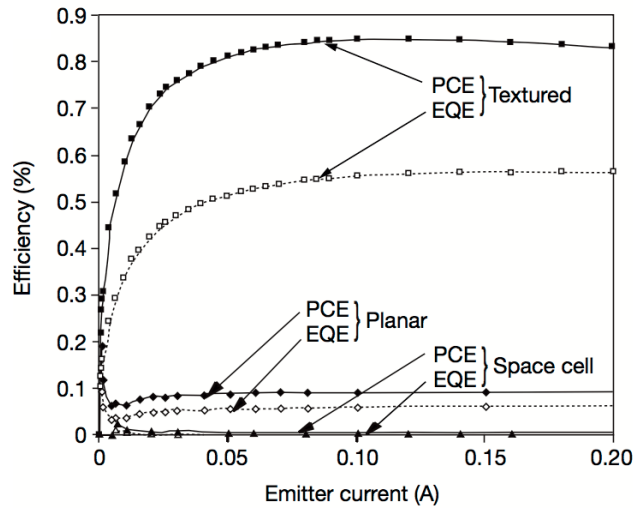


Figure 2.20. External quantum efficiency and power conversion efficiency as a function of diode current. Filled symbols and solid lines indicate power conversion efficiency (PCE); open symbols and dotted lines indicate external quantum efficiency (EQE). Squares, textured diode; diamonds, planar diode; triangles, high efficiency solar cell diode [13]. (See Appendix for documentation of permission to republish this material.)

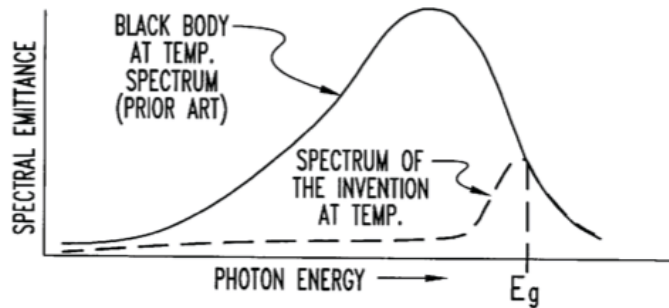


Figure 2.21. Graph showing the idealized relationship of the emittance spectrum of the silicon carbide invention with that of a standard blackbody [14]. (Source: United States Patent and Trademark Office, [www.uspto.gov](http://www.uspto.gov))

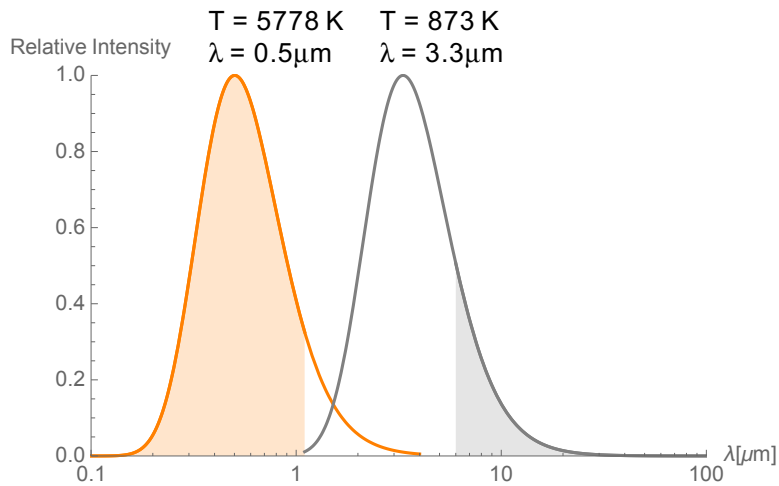


Figure 2.22. Simulated blackbody spectrum for the Sun (orange line,  $T = 5778 \text{ K}$ ) and an object at  $T = 600 \text{ }^{\circ}\text{C}$  (gray line,  $T = 873 \text{ K}$ ), with peak emission at  $\lambda = 0.5 \mu\text{m}$  and  $\lambda = 3.3 \mu\text{m}$ , respectively. The filled-in orange region represents the wavelengths with energy greater than silicon's absorption edge,  $1.1 \mu\text{m}$ . The filled-in gray region represents silicon's absorption edge for lattice vibrations,  $> 6 \mu\text{m}$ .

## 2.4 Solar Conversion Efficiency

Provided in the Woodall et. al. work was the framework to mathematically describe selective-absorber solar conversion efficiency [15]. For solar conversion efficiency, we have to consider two efficiencies. The first describes a material's ability to absorb and retain incoming radiation as heat. Factors that would reduce this efficiency are front surface reflections and total power emitted. Note that once an absorber reaches steady-state, the radiation-to-heat efficiency drops to zero. This diminished efficiency is due to all incoming optical power exiting the absorber as emission. The efficiency drop is demonstrated by

the black line in Fig. 2.23. Radiation to thermal-heat efficiency is given by,

$$\begin{aligned}\eta_{heat} &= \frac{P_{in} - P_{rad}}{P_{in}} \\ &= \frac{P_{in} - A\sigma\varepsilon(T^4 - T_0^4)}{P_{in}} \\ &= 1 - \frac{A\sigma\varepsilon(T^4 - T_0^4)}{P_{in}}.\end{aligned}\tag{2.10}$$

The second efficiency we need to consider converts captured thermal heat into work. The Carnot efficiency is invoked for this conversion of an ideal case,

$$\eta_{Carnot} = 1 - \frac{T_0}{T_H}.\tag{2.11}$$

The total solar conversion efficiency is a product of these two efficiencies,  $\eta_{Total} = \eta_{Heat} \times \eta_{Carnot}$ . The metric measures captured photothermal power available to do work. Efficiency is small at low temperatures because of poor Carnot efficiencies. At elevated temperatures, efficiency decreases due to absorber emission scaling proportional to  $T^4$ . The product of two effects are demonstrated by the orange line in Fig. 2.23. The total solar conversion efficiency is given by,

$$\eta_{Total} = \left(1 - \frac{A\sigma\varepsilon(T^4 - T_0^4)}{P_{in}}\right) \left(1 - \frac{T_0}{T}\right).\tag{2.12}$$

For a desired operating temperature and input power, the peak solar efficiency coincides with the maximum of Eq. 2.12. Solar conversion efficiency is optimized at moderate concentrations because operating temperature depends on optical input power. At low concentrations, absorber operating temperatures for Carnot efficiency are too low and yield low solar conversion. At high concentrations ( $>100X$ ), peak efficiency can be detrimental by corresponding to temperatures above the absorber's melting point. Figure 2.24 shows an ideal selective absorber coupled to a heat engine reaches efficiencies greater than 50% at moderate concentrations (100X) of solar flux, outperforming a blackbody coupled to a heat engine.

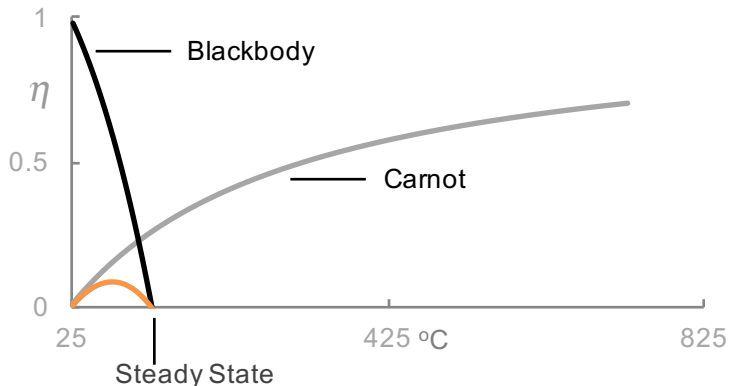


Figure 2.23. Simulation of efficiencies at 1 sun. Blackbody absorption efficiency performs better at low temperatures; Carnot efficiency, at elevated temperatures. Once the blackbody reaches steady-state temperature it emits all incoming power. The orange line represents the product of both efficiencies.

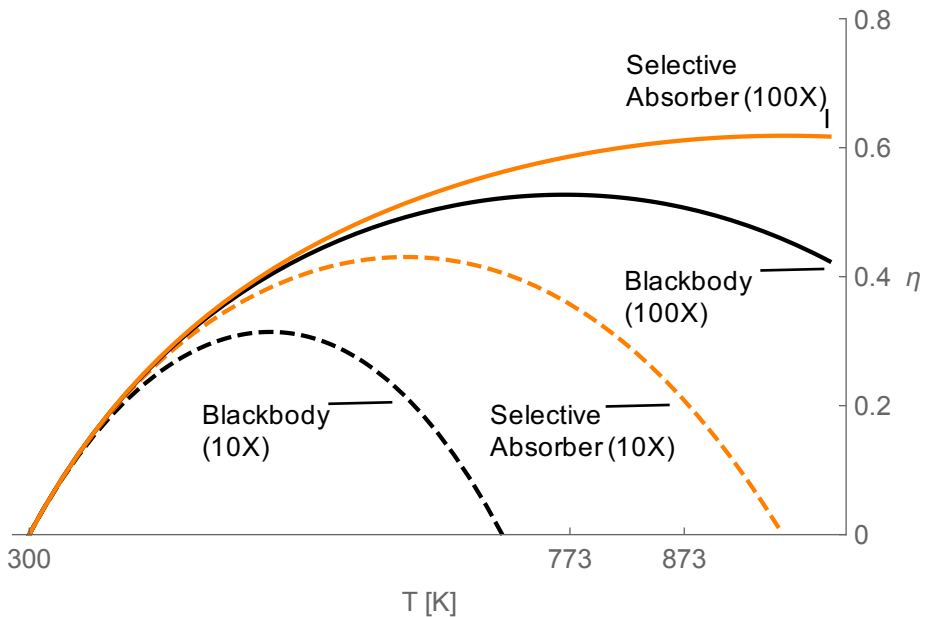


Figure 2.24. An ideal selective absorber and blackbody measured for solar conversion efficiency as a function of temperature. For 100X, peak selective absorber ( $\varepsilon = 0.3$ ) efficiency occurs near  $T = 873$  K (600 °C).

## 2.5 Levelized Cost Of Electricity

Today we have many methods for generating electricity, with many sources of fuel ranging from coal to biogas to solar radiation. Because of the numerous methods to generate electricity, a simple metric is needed to compare them to one another. The metric needs to consider the upfront cost of the system and fuel and maintenance, all over the lifetime

total of electricity generated—that is the leveled cost of electricity (LCOE) given by,

$$\begin{aligned} \text{LCOE} &= \frac{\text{Lifetime cost}}{\text{Lifetime energy produced}} \\ &= \frac{\sum_{t=1}^n \frac{I_t + M_t + F_t}{(1+r)^t}}{\sum_{t=1}^n \frac{E_t}{(1+r)^t}} \left[ \frac{\$}{kWhr} \right] \end{aligned} \quad (2.13)$$

where  $I_t$  is investment costs,  $M_t$  is maintenance costs,  $F_t$  is fuel costs,  $E_t$  is electrical energy generated,  $r$  is discount rate, and  $n$  is expected lifetime of system [16]. This is a general version of the LCOE which includes a discount rate, a tool used to calculate the net present value of a future venture. This LCOE discounts energy and costs; even though PV plants have relatively short install time, the overnight LCOE cost component greatly depends on the discount rate.

The solar harvester LCOE version parameters are given per unit area:

$$\text{LCOE} = \frac{C_{Cell} + C_{BOS} + C_{Inst}}{P_S \eta f_S L_S} \left[ \frac{\$}{kWhr} \right]. \quad (2.14)$$

where  $C_{Cell}$  is cell costs,  $C_{BOS}$  is balance of system costs,  $C_{BOS}$  is installation costs,  $P_S$  is solar power density,  $\eta$  is system efficiency,  $f_S$  fraction of time at full solar power, and  $L_S$  system lifetime.

LCOE compares all generation systems in  $\$/kWh$ , regardless of fuel source. This metric is useful when comparing expensive and efficient power plants that have a lifetime of 20 years to inexpensive novel technologies like organic solar cells with lifetimes of a 1/2 year. It was worth noting, a system with a lifetime of 1/2 year would have to purchased multiple times over to match the power output of the former. Table 2.3 and Table 2.4 are examples of LCOE across different technologies, e.g. dispatchable versus non-dispatchable energy sources. According to the U.S. Energy Information Agency, Geothermal is the most cost effective dispatchable energy source (Table 2.3). Wind is the most cost effective non-dispatchable energy source (Table 2.4).

Table 2.3. Most common dispatchable U.S. average capacity leveled costs (2013 \$/MWh) for plants entering service in 2020 [17].

Plant Type	Capacity Factor [%]	LCOE
Conventional Coal	85	95.1
Natural Gas	87	75.2
Advanced Nuclear	90	95.2
Geothermal	92	47.8
Biomass	83	100.5

Table 2.4. Most common non-dispatchable U.S. average capacity leveled costs (2013 \$/MWh) for plants entering service in 2020 [17].

Plant Type	Capacity Factor [%]	LCOE
Wind	36	73.6
Wind-Offshore	38	196.9
Solar PV	25	125
Solar Thermal	20	239.7
Hydroelectric	54	83.5

It should also be noted that LCOE is not the only metric considered when making additions to energy portfolios. For example, the leveled avoided cost of electricity with respect to current technology should be acknowledged as well. Also, the capacity factor, seen in Table 2.3 and Table 2.4, means different things for different technologies: For PV or Wind it is the time natural resources are available to produce power; for fossil fuel plants capacity factor refers to the time a certain generator is run. Consequently, for traditional power plants, a variable capacity factor is a strength because it adjusts to peak load demand. Adjusting to peak demand is another factor that is a potential challenge with an influx of solar energy contributing to overgeneration. As more PV comes online overgeneration becomes a risk, visualized in The Duck Chart (Fig. 2.25). The chart confirms that without a storage solution, no singular technology will solve our energy needs. The energy solution will have to be an aggregate of economical and storage

ready technologies. Other factors that play a role on future projects are policy, subsidies, and non-economic drivers.

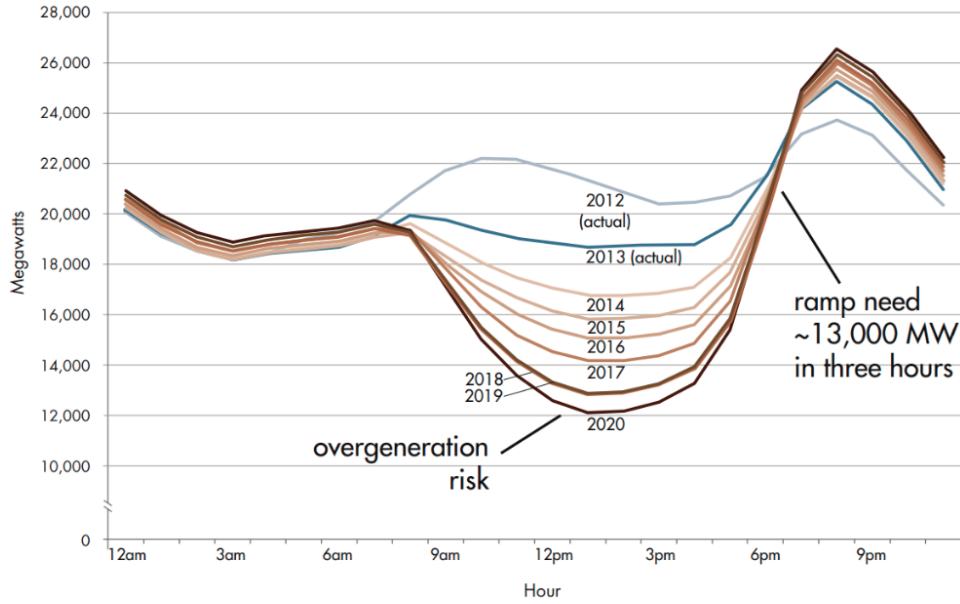


Figure 2.25. The CAISO Duck Chart identifies an overgeneration risk. The plot exemplifies the challenge of balancing dispatchable and non-dispatchable power [18]. This plot is courtesy of the National Renewable Energy Laboratory, Golden, CO. (As a work of the U.S. federal government, the image is in the public domain in the United States. P. Denholm, M. O'Connell, G. Brinkman, and J. Jorgenson, "Overgeneration from Solar Energy in California: A Field Guide to the Duck Chart," National Renewable Energy Laboratory, Tech. Rep. NREL/TP-6A20-65023, Nov, 2015.).

# Chapter 3

## Materials and Methods

Everybody has a plan  
until they get punched in the face

---

*Iron Mike Tyson*

In order to extrapolate emissivity from temperature readings, an intimate contact between intrinsic silicon and a thermocouple was needed. Spot welding a fine thermocouple to silicon samples for temperature readout was originally intended. However, because intrinsic silicon behaves like an insulator, spot welding provided a challenge. The challenge was overcome by using a highly conductive silver epoxy to bond samples and thermocouples. The author was relieved. To accurately measure total hemispherical emissivity, samples also needed a thermally isolated environment. In order to limit background radiation and convection, a custom vacuum chamber was designed.

### 3.1 Materials

The interior of the chamber was coated with high-temperature, high emissivity, paint. The black paint minimizes reflections and maximizes sample radiant cooling. A diaphragm pump brought the chamber down to low pressures,  $\sim$ 3mTorr. A convection vacuum gauge measured chamber pressures and relayed them to a digital display. A Xenon arc lamp provided a broad spectrum of radiation, with a color temperature approximating sunlight in the visible wavelengths. The input optical power passed through a glass convex lens.

The lens focused the input beam diameter from 1 inch to 1cm, see Fig. 3.2. The radiation then passed through a view port made of Kodiak glass, with refractive index  $n = 1.487$ . Kodiak glass was used because of high transmission for the visible spectrum, 90%. Testing in the laboratory verified the glass attenuated the Xenon arc lamp ( $15 \text{ W/cm}^2$ ) by 10%. Finally, the focused beam irradiated a piece of intrinsic silicon. (A list of components and materials used can be found in Appendix Table C.1.)

## 3.2 Sample Preparation

By definition, intrinsic silicon, also called undoped silicon, contains an equal amount of excited electrons as holes. The carrier densities directly relate to conductivity and resistivity,  $1/\rho = \sigma$  and

$$\sigma = q(\mu_n n + \mu_p p), \quad (3.1)$$

where  $q$  is electron charge,  $\mu_n$  is electron mobility,  $n$  is electron density,  $\mu_p$  hole mobility, and  $p$  hole is hole density. (See Fig. C.1 for intrinsic silicon's carrier concentration temperature response.) The sample of intrinsic silicon used in this work had a resistivity of  $2.0 \times 10^5 \Omega\text{cm}$  (Table 3.1). (For reference, glass has resistivity of  $10^{14} \Omega\text{cm}$ ; copper,  $1.7 \times 10^{-6} \Omega\text{cm}$ .) With this large resistivity silicon behaves like an insulator. Thus, making it difficult to attach a thermocouple by spot-welding, a process that fuses metal surfaces using electric current resistive heat. In a failed attempt to generate more carriers, one sample was pre-heated before spot-welding.

Instead, thermocouples were successfully mated to samples with a small bead of silver epoxy. To improve adhesion, before epoxy application, a small sample section was scuffed with sandpaper. The beads set at room temperature for 1-2 hours. The set samples were then heated and cured for 2 hours in a furnace, at  $200^\circ\text{F}$  (Fig. 3.1). The silver epoxy method was preferred because it successfully bonded the sample and thermocouple, and served as an efficient thermal conductor.

Table 3.1. Resistivity for silicon wafers used in the previous art compared to an intrinsic wafer for this work. This work used an intrinsic wafer which translates to high resistivity and low conductivity.

	$\rho$ [ $\Omega\text{cm}$ ]	$\sigma$ [ $\text{Scm}^{-1}$ ]
This work	20000	5.0E-05
Sato [7]	0.007	1.4E+02
	15	6.7E-02
Jain [19]	600	1.7E-03
	14	7.1E-02
	0.1	1.0E+01
	0.04	2.5E+01
Vandenabeele [20]	50	2.0E-02
Timans [8]	0.012	8.3E+01
	70	1.4E-02
Sugawara [21]	10	1.0E-01

### 3.3 Measurement Protocol

After the silver epoxy cured in the furnace, samples were suspended in the vacuum chamber (Fig. 3.3). Once secured, the roughing pump pulled down a vacuum,  $\sim 3$  mTorr. Then, the lamp beam spot was focused onto the sample by making small adjustments to the chamber and beam position (Fig. 3.2 and Appendix Fig. C.3). The thermocouple relayed specimen temperature readings to a multimeter, while a LabView script recorded measurements at 500 ms intervals.

### 3.4 Solving for Emissivity

With recorded temperature responses, emissivity can be solved for in one of four ways:

- (1) On the initial temperature ramp up, position **a** in Fig. 3.4. However, this happens in microseconds, which makes it difficult to gather enough data, and it assumes knowledge of input optical power. The input optical power can drift over this short time period.
- (2) The sample reaches maximum temperature in the steady-state region, relative to



Figure 3.1. K-type thermocouple adhered to isostatic graphite (1 in x 1 in). Heredia, C., 2015. [photograph]

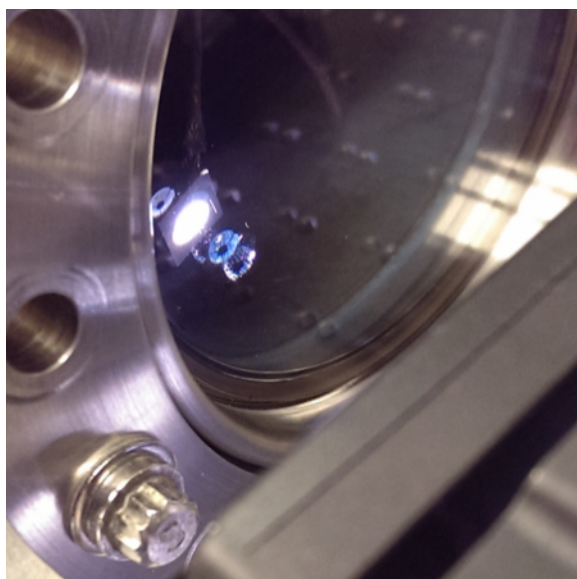


Figure 3.2. Xenon beam focused onto sample (1 cm x 1 cm) through viewport. Heredia, C., 2015. [photograph].

input power, position **b** in Fig. 3.4. Here, the Stefan-Boltzmann equation can be used to extrapolate for emissivity, but this assumes knowledge of input power. (3) Again in the steady-state region, by taking the temperature ratio of the sample to that of a blackbody. No knowledge of input power needed. (4) In the thermal decay region (no incoming input power), position **c** in Fig. 3.4, following the same thermal decay protocol as Woodall et

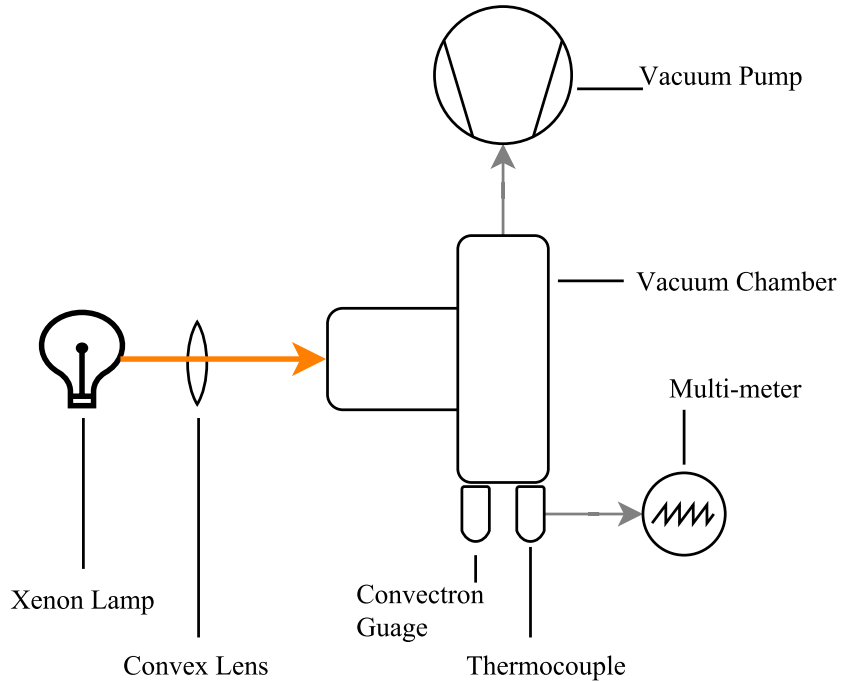


Figure 3.3. Schematic of the experimental setup. The optical power source is a Lambda LS Xenon lamp. Radiation enters the vacuum chamber through a Kodiak glass view port. A Convection gauge monitors the internal pressure of the chamber, which is pumped down with a roughing pump. Real time temperature output is measured from the K-type thermocouple by a Keithley multi-meter. The multi-meter communicates with a computer running a Labview script which records temperature readings over time.

al. [2].

### 3.4.1 Solving For Emissivity Relative To A Blackbody

This calculation is useful when input power is unknown. From conservation of energy, solving for effective emissivity from steady-state temperatures. For a blackbody, the input optical power flux equals the radiated power flux, that is:

$$P_{in} = P_{out}$$

$$A_{1,B}F_0 = A_{2,B}\varepsilon_0\sigma(T_B^4 - T_0^4) \quad (3.2)$$

where the area  $A_{1,B}$  represents the area irradiated by the initial power flux,  $F_0$ , the area  $A_{2,B}$  represents the area of power radiating through Stefan-Boltzmann Law,  $T_B$  and  $T_0$  represent blackbody and room temperature, respectively. For large  $A_{2,B}$ ,  $T_B$  must decrease, as expected, since there is more surface area to radiate power away. Conversely,

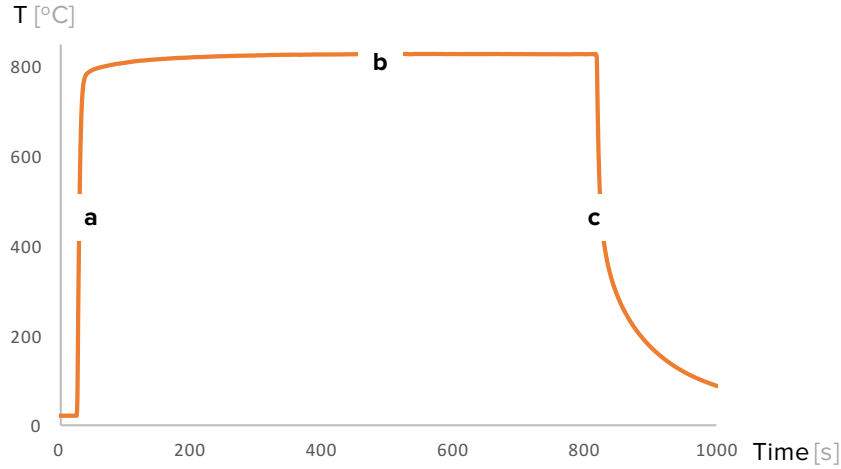


Figure 3.4. Experimental result: temperature response curve of a heated sample. At position **a** the radiation source is on and the substrate begins to heat up. Steady state temperature is reached at position **b**. Position **c**, source off, the substrate begins to cool down by emission; thermal decay equations are used to solve for emissivity.

if  $A_{2,B}$  is small, then  $T_B$  must increase to compensate, due to less surface area radiating power away. Moreover, since a blackbody emits and absorbs perfectly over all wavelengths,  $\varepsilon = 1$ . Therefore:

$$P_{out} = A_{2,B}\sigma(T_B^4 - T_0^4) [W] \quad (3.3)$$

For a heated sample a fraction of incident power reflection is expected. This fraction can be taken into account by the reflected and absorbed power given by  $RF_0$  and  $(1-R)F_0$ , respectively. Equation 3.2 can then be modified as:

$$\begin{aligned} P_{in} &= P_{out} \\ A_{1,S}(1 - R)F_0 &= A_{2,S}\varepsilon\sigma(T_S^4 - T_0^4) \end{aligned} \quad (3.4)$$

If area, reflectivity, and steady-state temperature were measured for a given radiation flux,  $F_0$ , then conservation of energy yields two equations, Eq. 3.3 and Eq. 3.4, with two unknowns— $\varepsilon$  and  $F_0$ . Assuming the same initial conditions for the heated object's emissivity,

$$\begin{aligned} \frac{A_{2,B}}{A_{1,B}}(1 - R)\sigma(T_B^4 - T_0^4) &= \frac{A_{2,S}}{A_{1,S}}\varepsilon\sigma(T_S^4 - T_0^4) \\ \varepsilon &= \frac{A_{1,S}}{A_{2,S}} \frac{A_{2,B}}{A_{1,B}}(1 - R) \frac{T_B^4 - T_0^4}{T_S^4 - T_0^4} \end{aligned} \quad (3.5)$$

For equal absorbed to radiated area ratios, emissivity simplifies to

$$\varepsilon = (1 - R) \frac{T_B^4 - T_0^4}{T_S^4 - T_0^4} \quad (3.6)$$

and for temperatures where  $T_B \gg T_0$ , and equivalent area ratios, then emissivity simplifies to

$$\varepsilon \approx (1 - R) \left( \frac{T_B}{T_S} \right)^4. \quad (3.7)$$

This equation can be interpreted as a relative emissivity. An object with emissivity less than 1 will always be hotter than a blackbody, as shown in Fig. 2.12; decreasing the emissivity of a selective absorber increases its steady-state temperature. This calculation is useful when input power is unknown; and the ratio is the fundamental definition of emissivity.

### 3.4.2 Solving For Emissivity In The Thermal Decay Region

Again starting with conservation of energy, extrapolating emissivity from thermal decay:

$$\begin{aligned} P_{initial} &= P_{final} \\ \frac{mC_p(T)\Delta T}{\Delta t} &= A\varepsilon\sigma (T^4 - T_0^4) \end{aligned} \quad (3.8)$$

and

$$\varepsilon = \frac{mC_p(T)(\Delta T/\Delta t)}{A\sigma(T_0^4 - T_S^4)}. \quad (3.9)$$

This equation assumes knowledge of mass, heat capacity, and temperature decay over a period of time.

# Chapter 4

## Results

An experiment is a question which science poses to Nature, and a measurement is the recording of Nature's answer

---

*Max Planck*

Considerable evidence suggests that doped silicon, at high temperatures, has poor emissivity values ( $\geq 0.7$ ) for use as a selective absorber. Selective absorber efficacy for photothermal conversion is dependent on the absorbers total hemispherical emissivity. To determine emissivity we used the thermal decay method for graphite and intrinsic silicon. Our results suggest that in the absence of dopants in silicon, free carrier absorption minimally contributes to absorption and emission at wavelengths other than the band gap.

### 4.1 Solving For Emissivity

#### 4.1.1 Graphite

We used graphite as a blackbody reference with a known emissivity. Emissivity was evaluated using the thermal decay equation, Eq. 3.9. Because thermal decay depends on heat capacity, a temperature dependent heat capacity was tracked using known values [22] (Fig. 4.1). We separated the thermal decay data into three regions: 100 - 200,

300, and 300 - 400 °C (Fig. 4.2). The graphite emissivity results are in agreement with the data in the literature [23, 24], indicating that this work properly measured emissivity.

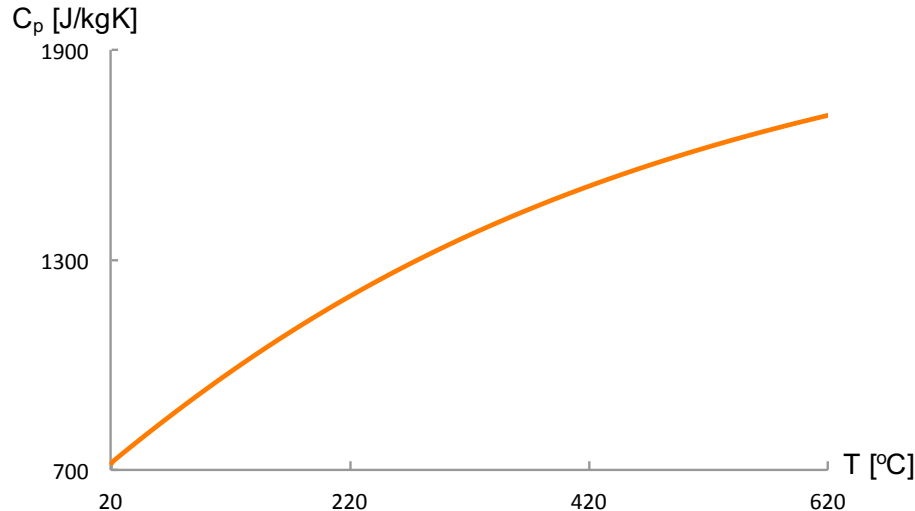


Figure 4.1. Graphite heat capacity increases with temperature. Plotted with data from ASTM International [22].

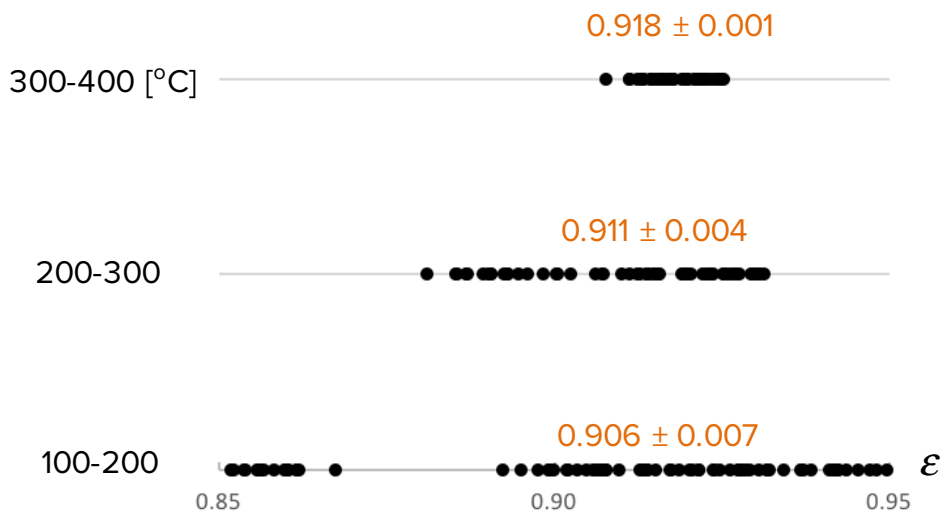


Figure 4.2. Graphite emissivity distribution for three temperature ranges: 100 - 200, 200 - 300, and 300 - 400 °C. The black dots represent datum points.

#### 4.1.2 Intrinsic Silicon

To characterize intrinsic silicon emissivity, we used the thermal decay method. Using data from Endo [25], heat capacity was mapped as a function of temperature (Fig. 4.3). We

separated the thermal decay data into six distributions ranges: 100 - 200, 200 - 300, 300 - 400, 400 - 500, 500 - 600, and 500 - 700 °C (Fig. 4.4). Results indicate that emissivity for undoped silicon remains low at elevated temperatures, 0.16 to 0.33 (Fig 4.5). These results suggest intrinsic silicon has selective absorber characteristics.

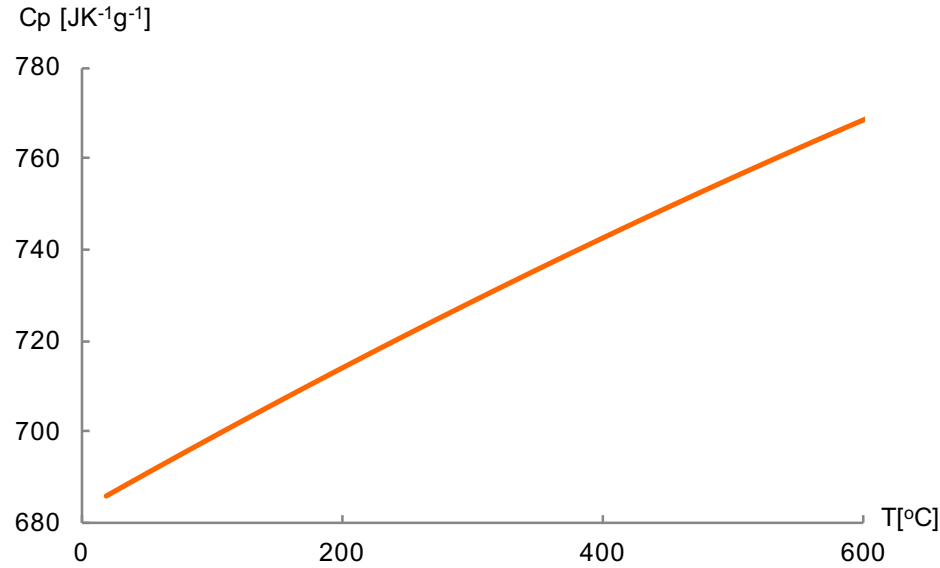


Figure 4.3. Intrinsic silicon heat capacity as a function of temperature. Plotted with data from Endo [25].

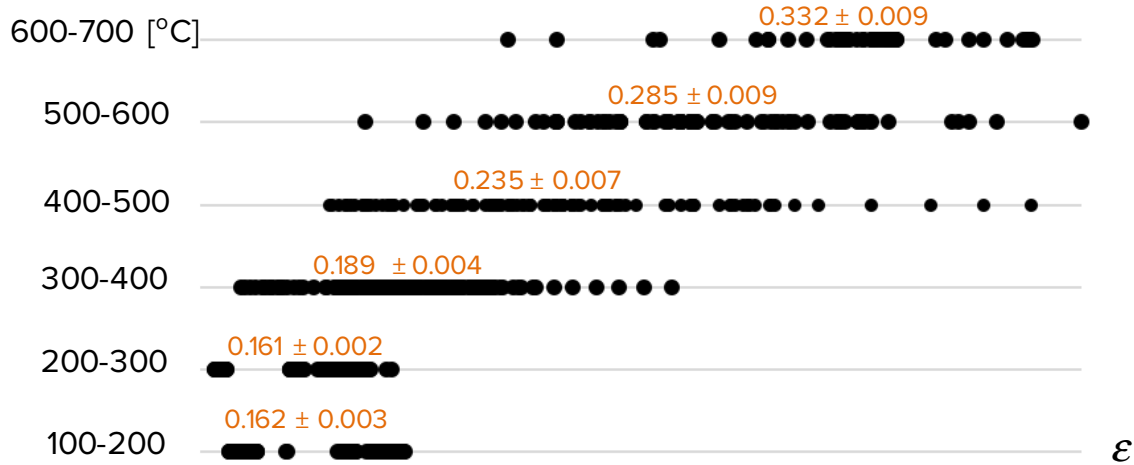


Figure 4.4. Intrinsic silicon emissivity distribution for temperature ranges from 100 to 700 °C. The black dots represent datum points.

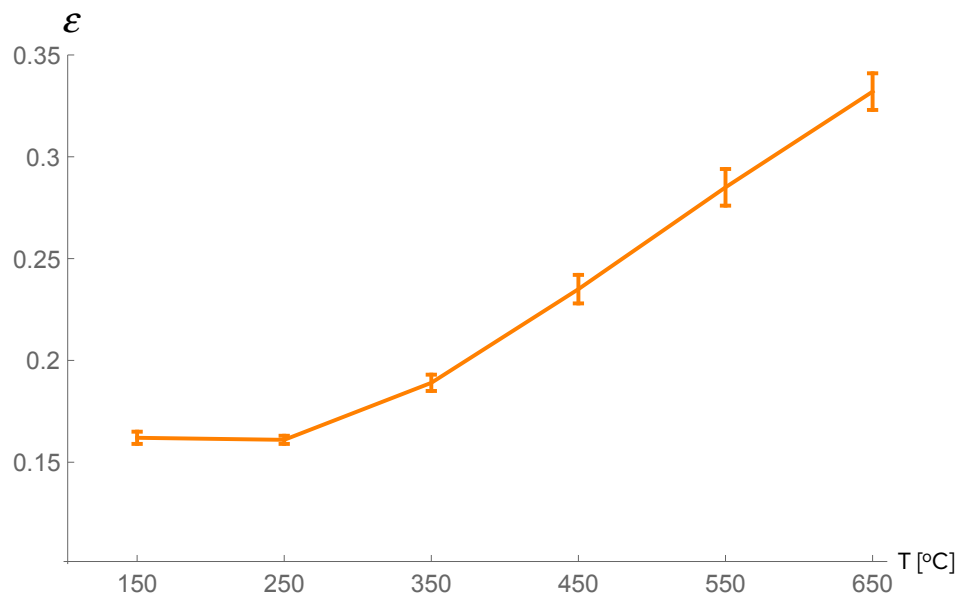


Figure 4.5. Intrinsic silicon emissivity plotted as a function of temperature.

# Chapter 5

## Discussion

In this study, we have shown that the emissivity of intrinsic silicon is low at elevated temperatures. We have identified three regions where emissivity could be extrapolated: heating, steady-state, and cooling. In the cooling region, emissivity was found using the thermal decay method. The thermal decay method measures total hemispherical emissivity by measuring the cooling rate through photon emission. The method delivered consistent results for both intrinsic silicon and graphite.

In our experiments for temperatures less than 300 °C, intrinsic silicon has a small emissivity (0.16). A small emissivity, at low temperatures, is consistent with previous low doped-silicon experiments [7, 8, 10, 11, 19, 20, 21, 24, 26, 27]. For elevated temperatures, to our surprise, unlike doped silicon, we discovered intrinsic silicon emissivity values remain low (Fig. 4.5). These results suggest no doping leads to minimal free carrier contributions, i.e. doping contributes to parasitic absorption and, hence, emission. According to the literature, free carriers lead to an increase in absorption and emission [7, 8]. We hypothesize the modest increase in emissivity (0.16 to 0.33) likely corresponds to an increase in carrier concentration with an increase in temperature (Appendix Fig. C.1). Note, an absorber with a temperature of 600 °C will have a peak blackbody emission at  $3.3 \mu m$ . At that temperature, silicon does not have a strong mechanism for emission. For silicon, band gap emission and absorption occurs at 1.12 eV or  $1.1 \mu m$  (Fig. 2.22). Hence, silicon will have a low emissivity at moderate temperatures.

The emissivity of isostatic graphite was consistent over the temperature range 100

- 400 °C,  $\varepsilon = 0.91$ . These results correspond to literature values for isostatic graphite [23, 24].

In summary, we used a thermal decay method to measure total hemispherical emissivity. Using this method, we measured the emissivity of intrinsic silicon for temperatures up to 700 °C. We observed low emissivity values for intrinsic silicon. Intrinsic silicon's low emissivity make it an ideal candidate for cost-effective photothermal conversion.

### 5.0.1 LCOE Revisited

Analysis of intrinsic silicon emissivity showed that it is well suited as a selective absorber. As an absorber it absorbs most of the solar radiation. The radiation subsequently converted to heat is preserved as heat by minimally emitting in the infrared wavelengths due to its low emissivity. By using this new emissivity data and estimating the cost of goods to build a photothermal generation system, we can calculate an LCOE (Table 5.1). The LCOE is an estimate for a 12-inch diameter SA ( $\varepsilon = 0.33$ ) operating at 700 °C and 16X. As a result, this LCOE bests all other non-dispatchable technologies (Table 2.4).

Using Table 2.2 to calculate the average power per square foot, we can then compare the average power footprint of PV and CSP and estimated SA generation. Since current commercial PV panels vary from 200 to 300 W, with standard dimensions of 65 by 39 inches, we assume an average power rating of 250 watts; for this calculation, we assume a generous PV system efficiency of 35% for one Sun. CSP footprint is calculated from Table 2.2. SA generator values are calculated using the specifics from the preceding paragraph. SA generation demonstrates value for locations where the land footprint is a concern (Table 5.2).

Table 5.1. Estimated LCOE for SA generation system.

Cost of Goods [\$]		Energy Produced	
Lens	175	Power density [kW/m <sup>2</sup> ]	16.62
Engine	5000	Hours of operation	20000
Wafer	100	Fraction of day peak	6
Chassis	300	Solar Efficiency	0.90
Labor	120	Carnot Efficiency	0.57
		Total Efficiency	0.51
Total	5695		
		LCOE [\$/MWhr]	33.32

Table 5.2. Power per square foot comparison for CSP, PV, and SA generation.

Technology	Power Density [W/sq.ft]
CSP	3.53
PV	14.2
SA generation	32.5

# Chapter 6

## Future Work

### 6.0.1 Optimizing Thickness

To further reduce material costs and the LCOE, the selective absorber thickness should be optimized. Thickness is optimized by using Beers Law, the ratio of transmitted power to incident power. Invoking Beer's law for transmittance,

$$\begin{aligned} I &= I_0 e^{-\alpha x} \\ T &= \frac{I}{I_0} \\ T &= e^{-\alpha x} \end{aligned} \tag{6.1}$$

where  $I$  is the transmitted power,  $I_0$  incident power, and  $\alpha$  the absorption coefficient. Examining the transmittance will determine how much material is necessary for complete power absorption. For a simplified version of the visible spectrum, we use Eq. 6.1 to evaluate ideal thickness using well known optical constants for red, green, and blue wavelengths [28] (Fig. 6.1). The high energy photons,  $\lambda = 450$  nm, are absorbed closer to the surface. For intrinsic silicon, an ideal depth of 10 - 20  $\mu m$  will absorb most of the visible spectrum photons. Effective optical thickness is doubled by applying a backside mirror. A highly reflective and thermally conductive mirror will also facilitate heat transfer.

### 6.0.2 Decreasing Effective Emissivity

A cold mirror (heat reflector), not to be confused with backside mirror, placed between the input optical power and selective absorber could lower emissivity by reflecting back longer

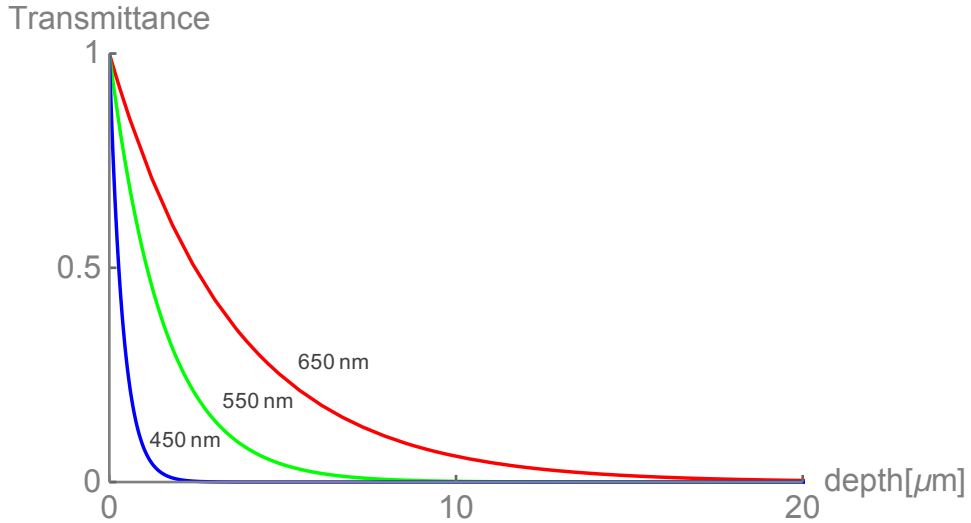


Figure 6.1. Simulation of intrinsic silicon transmittance for red (650 nm), green (550 nm), and blue (450 nm) wavelengths, with coefficients found in Green [28].

wavelengths. Another method could employ an oxide as an anti-reflective layer, such as Indium Tin Oxide or the more earth-abundant Fluorinated Tin Oxide, as a coating. These oxides have high transparency values and would reflect most of the infrared back into the selective absorber. This internally reflected and reabsorbed power would effectively lower the emissivity value.

Moreover, introducing a textured wafer surface, with a steepness of  $8 - 25^\circ$ , increases absorptance to greater than 90% [29]. The textured surface is formed by anisotropically etching inverted pyramids, exposing (111) equivalent crystallographic planes. The pyramids reduce reflections, and they increase absorptance of weakly absorbed photons within the wafer. The absorptance increases as light becomes randomized after internally reflecting from pyramids, a process known as light-trapping.

### 6.0.3 Finding Semiconductors Candidates

Why not use Germanium, it has a small band gap energy and can absorb more of the solar spectrum? Even though germanium's band gap is capable of absorbing most of the solar spectrum, its strength is its weakness. Because the band gap is so small, it would make for a great emitter of longer wavelengths. With a band gap of  $E_g = 0.66$  eV, its main mechanism for absorption and emission occurs at  $1.9 \mu m$ . In other words,

Table 6.1. Band gap energy of well studied semiconductors [5].

Material	Eg [eV]
Si	1.12
Ge	0.66
GaAs	1.42
InP	1.34

it has an excellent mechanism to emit at longer wavelengths. Referencing Wein's Law and Fig. 2.22 the peak blackbody emission wavelength at 600 °C occurs at  $3.3 \mu m$ . A similar quick analysis could be done on further potential selective absorber candidates, see Table 6.1 for a list of studied semiconductors band gaps. This peak wavelength analysis does not address the behavior of free carriers generated at elevated temperatures. For total hemispherical emissivity, a SA should be tested in a chamber similar to this work.

# Appendix A

## Planck's Law Derived

The blackbody spectrum needs a mathematical description to describe its finiteness and shape. The following section lays out that mathematical framework for that description. The derivation was relegated to the Appendix because it invokes esoteric topics such as:

- The de Broglie Wavelength
- Sinusoidal solutions to the Schrödinger equation in a box
- Taylor Series Expansion
- The relationship between energy and the frequency of a photon

Everything in the Universe glows with light from its own internal heat. Heat is the energy of the particles that make up an object. Accelerated charges produce electromagnetic radiation light. Thus, an object made of vibrating charge particles glows. The hotter an object, the faster the vibration. Thus, the average frequency of emitted photons increases with temperature. The surface temperature of the Sun produces more photons in the green-yellow part of the spectrum, hence, a perceived yellow Sun. Humans at 310 K produce infrared photons.

**Planck Constant** Equipartition theorem hints at the correct solution by stating energy is evenly distributed along all possible energy states. This simple postulate gives a relationship for the frequency of the photons produced by thermal motion, Rayleigh-Jeans

Law. The law describes the blackbody spectrum fairly well at low frequency. However, at high frequency, it maps intensity to infinite irradiance. This unrealistic solution is known as the Ultraviolet Catastrophe.

$$B_v = \frac{v^2 k T}{c^2} \left[ \frac{W}{m^2 Hz \cdot sr} \right] \quad (\text{A.1})$$

It appears the problem with Rayleigh-Jeans Law is that it allows infinitely small segments of energy through out the electromagnetic spectrum. Max Planck solved this problem by quantizing the lowest energy state,  $hf$ . This limited how much energy the high-frequency vibration could hold. The added term, the Bose-Einstein distribution, gives the distribution of energy emitted with respect to wavelength and temperature.

$$B_v = \frac{2hv^3}{c^2} \frac{1}{e^{\frac{hv}{kT}} - 1} \left[ \frac{W}{m^2 Hz \cdot sr} \right] \quad (\text{A.2})$$

Planck's Law also demonstrated as temperature increases the peak emission wavelength decreases. With the help of this equation, Einstein proved energy is quantized. The photoelectric effect yields  $E = hf$ . If we integrate Planck's Law as a function of frequency or wavelength, we get the Stefan-Boltzmann relationship:

$$P = A\varepsilon\sigma T^4 [W] \quad (\text{A.3})$$

The following is dedicated to deriving the Stefan-Boltzmann equation. Reader beware.

#### A.0.0.1 Modes in Box

Assuming we have a photon in a box, the sinusoidal solutions will yield the following wave vector in one direction will be  $k_i = \frac{2\pi}{\lambda_i} = \frac{\pi n}{L_i}$ . In three directions the wave vector is  $k^2 = \frac{\pi^2}{L^2} = \frac{\pi^2(n^2+l^2+m^2)}{L^2} = \frac{\pi^2 p^2}{L^2}$ .

#### A.0.0.2 Counting the Modes

Now we need the number of modes of oscillation in the interval  $\nu$  to  $d\nu$ . Since we are only concerned with positive values of  $n,l,m$  we'll take one-eighth of the sphere,  $4\pi p^2 dp$ . Also, since photons have two independent modes or polarizations the number of modes is doubled,

$$dN = (2) \left( \frac{1}{8} \right) 4\pi p^2 dp = \frac{L^3}{\pi^2} k^2 dk. \quad (\text{A.4})$$

Thus, per unit volume, the volume of states is

$$d\left(\frac{N}{V}\right) = \frac{8\pi}{c^3} \nu^2 d\nu. \quad (\text{A.5})$$

#### A.0.0.3 Average Energy Density

The Ultraviolet Catastrophe arises from assuming oscillator average energy,  $\bar{E} = kT$ . In this case the the energy density of radiation per unit frequency interval per unit volume is  $du = u(\nu)d\nu = \frac{8\pi}{c^3} \nu^2 \bar{E} d\nu$ , where  $u(\nu) = \frac{8\pi\nu^2 kT}{c^3}$  yields the Rayleigh-Jeans equation. The appropriate solution uses the Boltzmann distribution to determine the probability of state given a certain temperature,

$$p_n = \frac{e^{-E_n/kT}}{\sum_{j=0}^M e^{-E_j/kT}}. \quad (\text{A.6})$$

Above,  $p_n$  is the probability of state  $n$ ,  $E_n$  the energy of state  $n$ ,  $k$  the Boltzmann constant,  $T$  the temperature of the system and  $M$  is the number of states accessible to the system. Thus, the average energy can now be written as

$$\bar{E} = \sum_{n=0}^{\infty} E_n p_n = \frac{\sum_{n=0}^{\infty} E_n e^{-E_n/kT}}{\sum_{j=0}^{\infty} e^{-E_j/kT}} = \frac{\sum_{n=0}^{\infty} nh\nu e^{-E_n/kT}}{\sum_{j=0}^{\infty} e^{-E_j/kT}} = \frac{\sum_{n=0}^{\infty} nh\nu e^{-h\nu nkT}}{\sum_{j=0}^{\infty} e^{-h\nu nj/kT}}. \quad (\text{A.7})$$

Making the substitution,  $x = e^{-h\nu/kT}$ ,

$$\bar{E} = \frac{\sum_{n=0}^{\infty} nh\nu x^n}{\sum_{j=0}^{\infty} x^n} = \frac{h\nu(x + 2x^2 + 3x^3 + \dots)}{1 + x + x^2 + \dots} = \frac{h\nu x(1 + 2x + 3x^2 + \dots)}{1 + x + x^2 + \dots} \quad (\text{A.8})$$

At this point we need to invoke two familiar Taylor Series expansions,

$$\begin{aligned} \frac{1}{(1-x)} &= 1 + x + x^2 + \dots \\ \frac{1}{(1-x)^2} &= 1 + 2x + 3x^2 + \dots \end{aligned} \quad (\text{A.9})$$

Thus, the average energy can be written as

$$\bar{E} = h\nu \frac{e^{-h\nu/kT}}{1 - e^{-h\nu/kT}} = h\nu \frac{1}{e^{-h\nu/kT} - 1} \quad (\text{A.10})$$

We have demonstrated the number of modes in the frequency interval  $\nu$  to  $d\nu$  is  $\frac{8\pi\nu^2}{c^3} d\nu$  per unit volume. The energy density of radiation in this frequency range is

$$u(\nu) = \frac{8\pi h\nu^3}{c^3} \frac{1}{e^{-h\nu/kT} - 1} \left[ \frac{J}{m^3 nm} \right] \quad (\text{A.11})$$

### A.0.1 Stefan-Boltzmann Law Derived

By integrating with respect to frequency, we can solve for flux as a function of temperature,  $I(T)$ . This is the Stefan-Boltzmann relationship.

$$\begin{aligned}
 I &= \int_0^\infty u(v)dv \\
 &= \int_0^\infty \frac{8\pi h\nu^3}{c^3} \frac{1}{e^{-h\nu/kT} - 1} dv \\
 &= \frac{8\pi h}{c^3} \int_0^\infty \frac{\nu^3}{e^{-h\nu/kT} - 1} dv
 \end{aligned} \tag{A.12}$$

Making the substitution  $x = -hv/kT$ ,  $dx = -h/kTdv$

$$\begin{aligned}
 I &= \frac{8\pi h}{c^3} \int_0^\infty \frac{-kT}{h} \left( \frac{-kT}{h} \right)^3 \frac{x^3}{e^x - 1} dx \\
 &= \frac{8\pi}{c^3 h^3} (kT)^4 \int_0^\infty \frac{x^3}{e^x - 1} dx
 \end{aligned} \tag{A.13}$$

Invoking another Taylor Series expansion, we can rewrite the integral as

$$\int_0^\infty \frac{x^3}{e^x - 1} dx = \int_0^\infty x^3 \frac{e^{-x}}{1 - e^{-x}} dx = \int_0^\infty x^3 \sum_{n=1}^\infty e^{-nx} dx \tag{A.14}$$

Making the substitution  $y = nx$ ,  $dy = n dx$ , we solve the integral

$$\begin{aligned}
 \int_0^\infty x^3 \sum_{n=1}^\infty e^{-nx} dx &= \sum_{n=1}^\infty \int_0^\infty \frac{y^3}{n^4} e^{-y} dy \\
 &= \sum_{n=1}^\infty \frac{1}{n^4} [e^{-y} (y^3 + 3y^2 + 6y + 6)]_0^\infty \\
 &= 6 \sum_{n=1}^\infty \frac{1}{n^4} \\
 &= 6 \frac{\pi^4}{90} \\
 &= \frac{\pi^4}{15}
 \end{aligned} \tag{A.15}$$

Finally, we can solve for the flux,

$$I = \frac{8\pi}{c^3 h^3} (kT)^4 \frac{\pi^4}{15} = \left( \frac{8\pi^5 k^4}{15 c^3 h^3} \right) T^4 \quad (\text{A.16})$$

Now we can solve for hemispherical power emitted as a function of temperature,

$$\begin{aligned} P &= \frac{A}{4\pi} \int_0^{2\pi} \int_0^{\pi/2} I \cos \theta \sin \theta d\theta d\varphi \\ &= \frac{A}{4\pi} I \pi = \frac{AI}{4} \\ &= A \left( \frac{2\pi^5 k^4}{15 c^3 h^3} \right) T^4 \\ &= A\sigma T^4 [\text{W}] \end{aligned} \quad (\text{A.17})$$

The term in parenthesis is the Stefan-Boltzmann constant,  $\sigma = 5.67 \times 10^{-8} \text{ Js}^{-1} \text{ m}^{-2} \text{ K}^{-4}$ .

## Appendix B

# Theoretical Solar Efficiency Limit

What is the maximum solar energy conversion? How much can we use for work? Assuming solar heat ( $Q_H$ ) flows from the solar surface at a temperature ( $T_H$ ) through the working substance (Fig. B.1). Then, the remaining heat ( $Q_C$ ) flows into the cold sink ( $T_C$ ). This heat flow forces the working body to do mechanical work ( $W$ ), i.e.  $W$  is used to convert solar power to electricity.  $\Delta S_G$  is the entropy generated in the conversion,  $\Delta S_G \geq 0$ . We can derive the solar efficiency (Eq. B.1) using the first and second laws of thermodynamics,

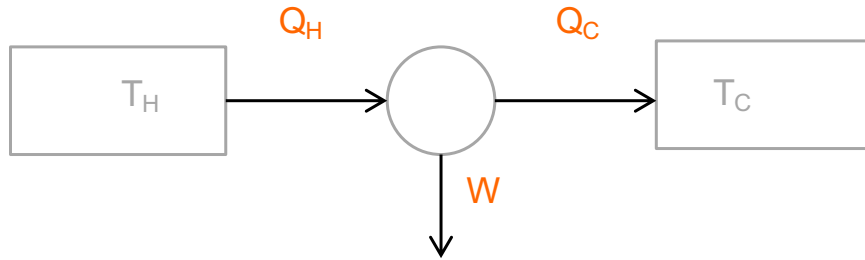


Figure B.1. Heat flow diagram for a converter which receives heat from a source ( $T_H$ ), and exhausts heat into a reservoir ( $T_C$ ).

$$1\text{st Law : } Q_H = W_{\text{converter}} + Q_C$$

$$2\text{nd Law : } \frac{Q_H}{T_H} + \Delta S_H = \frac{Q_C}{T_C}$$

$$\eta = \frac{W_{\text{converter}}}{Q_H} = 1 - \frac{T_C}{T_H} \quad (\text{B.1})$$

This is the Carnot efficiency. For solar temperatures, the Carnot efficiency is 95%. Because the converters entropy flux and radiation emitted are not considered, this efficiency

is not possible for solar energy conversion. The Landsberg limit accounts for entropy generation during the absorption and conversion processes. For solar photothermal conversion the first and second laws of thermodynamics become

$$1\text{st Law : } P_{Sun} = \dot{W}_{converter} + \dot{Q}_{converter} + P_{radiation}$$

$$2\text{nd Law : } \frac{4}{3} \frac{P_{Sun}}{T_{Sun}} + \Delta \dot{S}_G = \frac{4}{3} \frac{P_{radiation}}{T_{converter}} + \frac{\dot{Q}_{converter}}{T_C}$$

where  $\Delta \dot{S}_{Sun} = \int \frac{\partial T P_{Sun}}{T} dT = \frac{4}{3} \frac{P_{Sun}}{T_{Sun}}$  is the entropy flux for solar emission,  $\dot{W}_{converter}$  is the power converted to electricity,  $\dot{Q}_{converter}$  is the power used to heat the converter, and  $P_{radiation}$  is the power emitted by the converter.

$$\eta = 1 - \frac{4}{3} \frac{T_C}{T_H} + \left( \frac{T_{converter}}{T_H} \right)^4 \left( \frac{4}{3} \frac{T_C}{T_{converter}} - 1 \right) \quad (\text{B.2})$$

For solar temperatures and  $T_{converter} = T_C$ , this has a maximum efficiency of 93.3%. However, due to kinetic conversion entropy generation, efficiency maxes out at 86% [30].

# Appendix C

## Supplemental Material

Table C.1. Specifications of components in this work

Item	Specification	Model Number
6" Standard Tee	304L stainless steel tubing	T-0600
Convectron guage	10E-4 to 1000 Torr	KJL275196
Gauge Controller	10E-4 to 1000 Torr	KJL375011BA
Custom UHV Flange	(3) QF25 Welded in ports	CF-130515A
Vacuum pump	Down to 1E-4 Torr	2008A
Silver Epoxy	Up to 1200 °F	Pyro-Duct 597
Multimeter	5 1/2 Digit Multimeter	Model 2110
K-Type Thermocouple	-330 to 2460 °F	5TC-KK-K-30-72
Xenon Arc Lamp	320 to 700 nm, 300 W	Lambda LS 30
High Temp. Black paint	0.95 absorptivity	2500
Silicon wafer	FZ Intrinsic undoped Si: [111] +- 0.5 $R_o > 20,000 \text{ Ohmcm}$	C776
Isostatic graphite	High emissivity	IPG14

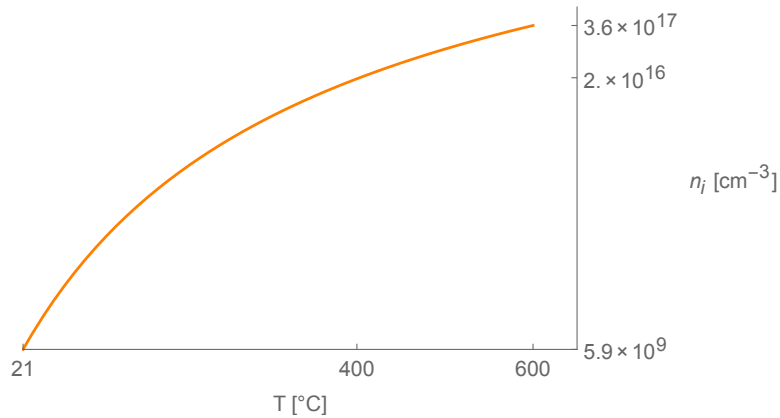


Figure C.1. Intrinsic carrier concentration as a function of temperature. The plot demonstrates carrier concentrations indeed depends on temperature. Plotted using data from Sproul [31].

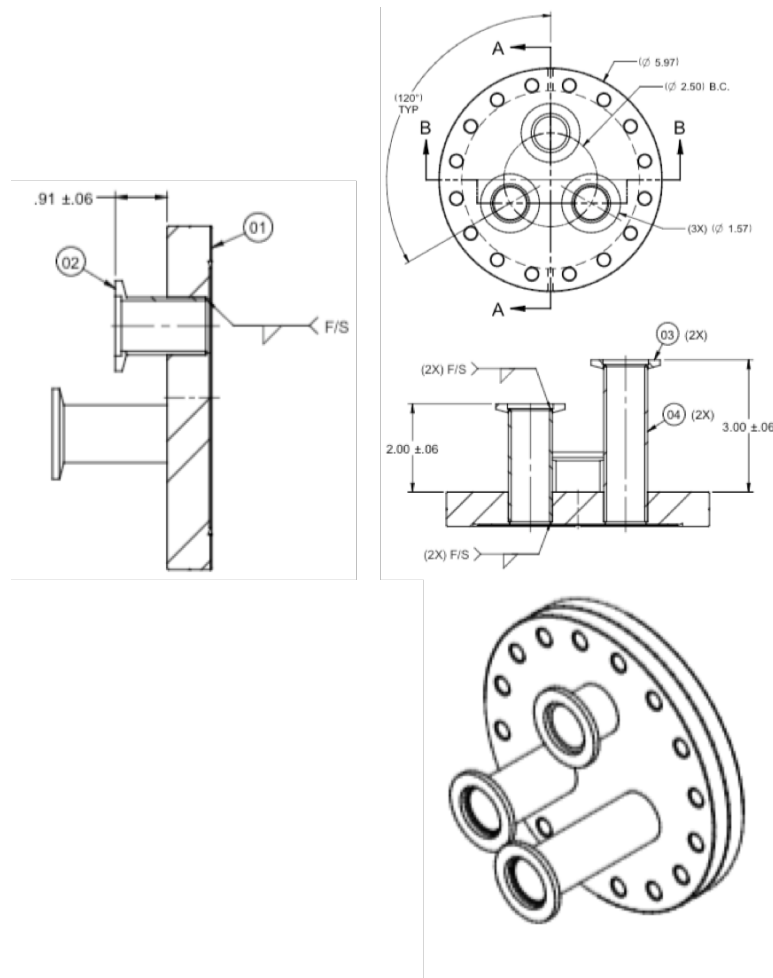


Figure C.2. Schematic of the custom flange and bisected side view of the chamber. The flange is essential because it allows a roughing pump connection, a thermocouple feedthrough, and convection gauge interfaced in one location. Heredia, C., 2015. [Drawing]

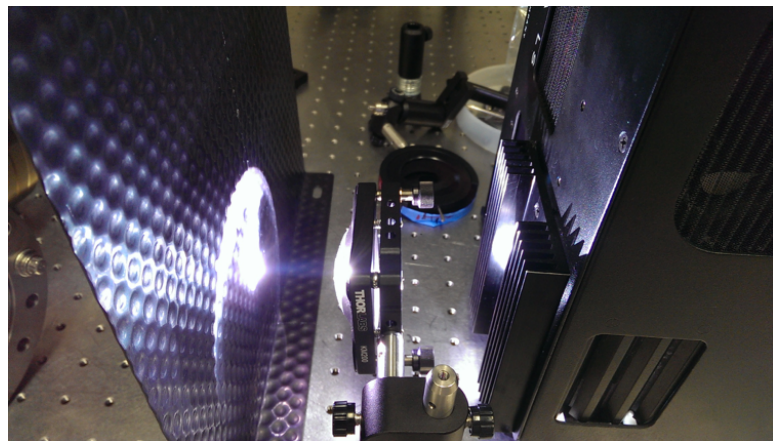


Figure C.3. Xenon beam focused onto backstop. Heredia, C., 2015. [photograph]

# **Appendix D**

## **Copyright Permissions**

This eBook is for the use of anyone anywhere at no cost and with almost no restrictions whatsoever. You may copy it, give it away or re-use it under the terms of the Project Gutenberg License included with this eBook or online at [www.gutenberg.org](http://www.gutenberg.org)

Title: The Theory of Heat Radiation

Author: Max Planck

Translator: Morton Masius

Release Date: June 18, 2012 [EBook #40030]

Language: English

Character set encoding: ISO-8859-1

AIP PUBLISHING LLC LICENSE  
TERMS AND CONDITIONS

Aug 16, 2016

---

This Agreement between Cristian A Heredia ("You") and AIP Publishing LLC ("AIP Publishing LLC") consists of your license details and the terms and conditions provided by AIP Publishing LLC and Copyright Clearance Center.

License Number 3931131328027

License date Aug 16, 2016

Licensed Content Publisher AIP Publishing LLC

Licensed Content Publication Journal of Applied Physics

Licensed Content Title Temperature dependence of the radiative recombination coefficient of intrinsic crystalline silicon

Licensed Content Author T. Trupke,M. A. Green,P. Würfel, et al.

Licensed Content Date Sep 30, 2003

Licensed Content Volume Number 94

Licensed Content Issue Number 8

Type of Use Thesis/Dissertation

Requestor type Student

Format Print and electronic

Portion Excerpt (< 800 words)

Will you be translating? No

Title of your thesis / dissertation Characterizing Silicon At High Temperatures: A Selective Absorber For Solar Energy Harvesting

Expected completion date Sep 2016

Estimated size (number of pages) 80

AIP PUBLISHING LLC LICENSE

TERMS AND CONDITIONS

Aug 17, 2016

---

This Agreement between Cristian A Heredia ("You") and AIP Publishing LLC ("AIP Publishing LLC") consists of your license details and the terms and conditions provided by AIP Publishing LLC and Copyright Clearance Center.

License Number 3931671364030

License date Aug 17, 2016

Licensed Content Publisher AIP Publishing LLC

Licensed Content Publication Applied Physics Letters

Licensed Content Title A new concept for solar energy thermal conversion

Licensed Content Author J. J. Cuomo,J. F. Ziegler,J. M. Woodall

Licensed Content Date Sep 2, 2008

Licensed Content Volume Number 26

Licensed Content Issue Number 10

Type of Use Thesis/Dissertation

Requestor type Student

Format Print and electronic

Portion Figure/Table

Number of figures/tables 1

Title of your thesis / dissertation Characterizing Silicon At High Temperatures: A Selective Absorber For Solar Energy Harvesting

Expected completion date Sep 2016

Estimated size (number of pages) 80

[Notice]

If you are the one of the authors of the paper, you don't have to apply for a permission with the following conditions.

1. Follow the Copyright Policy of the Japan Society of Applied Physics
2. A credit line of "Copyright (published year) The Japan Society of Applied Physics" should be added to the end of the figure caption in the Content.
3. The Content must be cited as a reference in the Publication.

---

To: President of the Japan Society of Applied Physics

29 / 8 / 2016  
Day Month Year

Submit to:  
Publication Center for Pure and Applied Physics, The Japan Society of Applied Physics  
2-31-22-5F, Yushima, Bunkyo-ku, Tokyo 113-0034, Japan  
TEL: +81-3-5844-3291 FAX: +81-3-5844-3290 E-mail address: permission@jsap.or.jp

Application for Permission to Reproduce Material

I request permission to reproduce the following material, copyrighted by the Japan Society of Applied Physics.

**Publication where material is reproduced (the Publication)**

Name of the Publication (e.g., journal title, book title): Characterizing Silicon at High Temperatures

Publisher (e.g., publishing company): Student Thesis (University of California, Davis.)

Planned date of publication: October 2016

Number of copies: Not applicable

**Content of reproduction (the Content)**

Journal title: The Japan Journal of Applied Physics

Volume/Year/ID(starting page): 6 / 1967 / 339

Article title: Spectral Emissivity of Silicon

Author(s): T.Sato

Content to be reproduced (please specify): Figure 1. Optical Arrangement

**Applicant (only to be completed by the author of the Publication)**

Name: Cristian Heredia

Affiliation (e.g., university, company, organization): University of California, Davis

E-mail address: caheredia@ucdavis.edu

---

I will abide by the following conditions of reproduction.

1. A credit line "Copyright publication year The Japan Society of Applied Physics" must be added to the Content (in the figure caption(s)). The material containing the Content, copyrighted by the Japan Society of Applied Physics, must be cited in the references of the Publication.
2. The Content will not be modified.
3. The Content will not be reproduced in other materials.

Signature of applicant: 

\* The purpose of reproduction will be considered before permission is granted.

---

**ENDORSEMENT**

Dr. Cristian Heredia

I permit the reproduction of the Content in the Publication.

30 / 08 / 2016

.....  
Day Month Year

President, The Japan Society of Applied Physics

Publication Center for Pure and Applied Physics, The Japan Society of Applied Physics

2-31-22-5F, Yushima, Bunkyo-ku, Tokyo 113-0034, Japan /TEL: +81-3-5844-3291/FAX: +81-3-5844-3290/E-mail address: permission@jsap.or.jp

Released March 2014

AIP PUBLISHING LLC LICENSE  
TERMS AND CONDITIONS

Aug 29, 2016

---

This Agreement between Cristian A Heredia ("You") and AIP Publishing LLC ("AIP Publishing LLC") consists of your license details and the terms and conditions provided by AIP Publishing LLC and Copyright Clearance Center.

License Number 3938461318183

License date Aug 29, 2016

Licensed Content Publisher AIP Publishing LLC

Licensed Content Publication Journal of Applied Physics

Licensed Content Title Emissivity of silicon at elevated temperatures

Licensed Content Author P. J. Timans

Licensed Content Date Nov 15, 1993

Licensed Content Volume Number 74

Licensed Content Issue Number 10

Type of Use Thesis/Dissertation

Requestor type Student

Format Print and electronic

Portion Figure/Table

Number of figures/tables 1

Title of your thesis / dissertation Characterizing Silicon At High Temperatures: A Selective Absorber For Solar Energy Harvesting

Expected completion date Sep 2016

Estimated size (number of pages) 80

August 17, 2016  
Cristian Heredia  
University of California, Davis  
Dear OSA Publishing:

I am completing a doctoral dissertation at the University of California, Davis entitled "Characterizing Silicon At High Temperatures: A Selective Absorber For Solar Energy Harvesting" I would like your permission to reprint in my dissertation excerpts from the following:

J. O. White, T. R. Kirst, and J. Tauc, "Amorphous silicon as a selective absorber of solar energy: a spectral emissivity study," Appl. Opt. **17**, 2427-2430 (1978)

The excerpts to be reproduced are:

"The absorption coefficient has little temperature dependence, and therefore it is unlikely that the absorption is due to free-carriers. This is true also in the region of longer wavelengths, where increases with wavelength as one would expect for free-carriers. We may speculate that this absorption is due to the high impurity content in the sample and is associated with the states in the gap; its increase at longer wavelengths may be due to a particular distribution of these states.

The residual absorption observed in these films makes them inefficient as selective absorbers for solar energy thermal convertors as discussed in Ref. 1. Besides argon, oxygen is the main impurity in these films, and one may speculate that oxygen is responsible for the residual absorption. "

The requested permission extends to any future revisions and editions of my dissertation, including non- exclusive world rights in all languages, and to the prospective publication of my dissertation by ProQuest through its ProQuest® Dissertation Publishing business. ProQuest may produce and sell copies of my dissertation on demand and may make my dissertation available for free internet download at my request. These rights will in no way restrict republication of the material in any other form by you or by others authorized by you. Your signing of this letter will also confirm that you own [or your company owns] the copyright to the above- described material.

If these arrangements meet with your approval, please respond in kind with a Permission License. Thank you very much.

Sincerely,  
Cristian Heredia

-----  
PhD Candidate, Department of Electrical and Computer Engineering University of California, Davis

Dear Cristian Heredia,

Thank you for contacting The Optical Society.

OSA considers your requested use of its copyrighted material to be Fair Use under United States Copyright Law. It is requested that the excerpt be clearly identified as a quotation and that a complete citation of the original material be included in any publication.

Kind Regards, Rebecca Robinson

Rebecca Robinson  
August 30, 2016  
Authorized Agent, The Optical Society

**NATURE PUBLISHING GROUP LICENSE  
TERMS AND CONDITIONS**

Dec 17, 2016

This Agreement between Cristian A Heredia ("You") and Nature Publishing Group ("Nature Publishing Group") consists of your license details and the terms and conditions provided by Nature Publishing Group and Copyright Clearance Center.

License Number 4011260135911

License date Dec 17, 2016

Licensed Content Publisher Nature Publishing Group Nature

Licensed Content Publication Licensed

Content Title Licensed Efficient silicon light-emitting diodes

Content Author Martin A. Green, Jianhua Zhao, Aihua Wang, Peter J. Reece and Michael Gal

Licensed Content Date Aug 23, 2001 412

Licensed Content Volume Number 6849

Licensed Content Issue Number reuse in a dissertation

Type of Use / thesis academic/educational

Requestor type print and electronic figures/tables/illustrations

Format

Portion

Number of figures/tables /illustrations 2

Figures Figure 2 and Figure 3 no

Author of this NPG article

Your reference number

Title of your thesis / dissertation Characterizing Silicon At High Temperatures: A Selective

Absorber For Solar Energy Harvesting

Expected completion date Sep 2016

Estimated size (number of pages) 80

Requestor Location

Cristian A Heredia 498 Johnston

WOODLAND, CA 95776 United States

Attn: Cristian A Heredia

Invoice

License Number 4014410828149  
License date Dec 22, 2016  
Licensed Content Publisher AIP Publishing LLC  
Licensed Content Publication Journal of Applied Physics  
Limiting efficiencies of ideal  
single and multiple energy gap  
terrestrial solar cells  
Licensed Content Author C. H. Henry  
Licensed Content Date Aug 1, 1980  
Licensed Content Volume 51  
Licensed Content Issue 8  
Requestor type Student  
Format Print and electronic  
Portion Figure/Table  
Number of figures/tables 2

## REFERENCES

- [1] M. Sivak, “Potential energy demand for cooling in the 50 largest metropolitan areas of the world: Implications for developing countries,” *Energy Policy*, vol. 37, pp. 1382–1384, Apr. 2009.
- [2] G. D. Pettit, J. J. Cuomo, T. H. Distefano, and J. M. Woodall, “Solar Absorbing Surfaces of Anodized Dendritic Tungsten,” *IBM Journal of Research and Development*, vol. 22, no. 4, pp. 372–377, 1978.
- [3] W. Shockley and H. J. Queisser, “Detailed Balance Limit of Efficiency of pn Junction Solar Cells,” *Journal of Applied Physics*, vol. 32, no. 3, pp. 510–519, 1961.
- [4] C. H. Henry, “Limiting efficiencies of ideal single and multiple energy gap terrestrial solar cells,” *Journal of Applied Physics*, vol. 51, pp. 4494–4500, Aug. 1980.
- [5] A. Polman, M. Knight, E. C. Garnett, B. Ehrler, and W. C. Sinke, “Photovoltaic materials: Present efficiencies and future challenges,” *Science*, vol. 352, Apr. 2016.
- [6] “Concentrated Solar Power Projects,” 2015.
- [7] T. Sato, “Spectral Emissivity of Silicon,” *The Japan Society of Applied Physics*, vol. 6, no. 3, p. 8, 1967.
- [8] P. J. Timans, “Emissivity Of Silicon At Elevated-Temperatures,” *Journal of Applied Physics*, vol. 74, pp. 6353–6364, Nov. 1993.
- [9] T. Trupke, M. A. Green, P. Wrfel, P. P. Altermatt, A. Wang, J. Zhao, and R. Corkish, “Temperature dependence of the radiative recombination coefficient of intrinsic crystalline silicon,” *Journal of Applied Physics*, vol. 94, no. 8, pp. 4930–4937, 2003.
- [10] J. O. White, T. R. Kirst, and J. Tauc, “Amorphous Silicon As A Selective Absorber Of Solar-Energy - Spectral Emissivity Study,” *Applied Optics*, vol. 17, no. 15, pp. 2427–2430, 1978.
- [11] N. M. Ravindra, B. Sopori, O. H. Gokce, S. X. Cheng, A. Shenoy, L. Jin, S. Abedrabbo, W. Chen, and Y. Zhang, “Emissivity measurements and modeling of silicon-related materials: An overview,” *International Journal of Thermophysics*, vol. 22, pp. 1593–1611, Sept. 2001.
- [12] P Wurfel, “The chemical potential of radiation,” *Journal of Physics C: Solid State Physics*, vol. 15, no. 18, p. 3967, 1982.
- [13] M. A. Green, J. Zhao, A. Wang, P. J. Reece, and M. Gal, “Efficient silicon light-emitting diodes,” *Nature*, vol. 412, pp. 805–808, Aug. 2001.
- [14] J. M. P. Woodall, K. T. Kornegay, and M. G. Spencer, “Incandescent light energy conversion with reduced infrared emission,” Sept. 1998.

- [15] J. J. Cuomo, J. F. Ziegler, and J. M. Woodall, “A new concept for solar energy thermal conversion,” *Applied Physics Letters*, vol. 26, no. 10, pp. 557–559, 1975.
- [16] M. Wittenstein and G. Rothwell, “Projected Costs of Generating Electricity,” tech. rep., Organisation for Economic Co-operation and Development/International Energy Agency, Paris, France, Sept. 2015.
- [17] “Annual Energy Outlook 2015,” Tech. Rep. DOE/EIA-0383(2015), U.S. Energy Information Administration, Apr. 2015.
- [18] P. Denholm, M. O’Connell, G. Brinkman, and J. Jorgenson, “Overgeneration from Solar Energy in California: A Field Guide to the Duck Chart,” *National Renewable Energy Laboratory, Tech. Rep. NREL/TP-6A20-65023, Nov*, 2015.
- [19] S C Jain and S K Agarwal and W N Borle and S Tata, “Total emissivity of silicon at high temperatures,” *Journal of Physics D: Applied Physics*, vol. 4, no. 8, p. 1207, 1971.
- [20] P. Vandenabeele and K. Maex, “INFLUENCE OF TEMPERATURE AND BACK-SIDE ROUGHNESS ON THE EMISSIVITY OF SI WAFERS DURING RAPID THERMAL-PROCESSING,” *Journal of Applied Physics*, vol. 72, pp. 5867–5875, Dec. 1992.
- [21] H. Sugawara, T. Ohkubo, T. Fukushima, and T. Iuchi, “Emissivity measurement of silicon semiconductor wafer near room temperature,” in *SICE 2003 Annual Conference (IEEE Cat. No.03TH8734)*, vol. 2, pp. 2201–2204 Vol.2, Aug. 2003.
- [22] “Practice for Testing Graphite and Boronated Graphite Materials for High-Temperature Gas-Cooled Nuclear Reactor Components,” tech. rep., ASTM International, 2014.
- [23] A. V. Kostanovskii, M. G. Zeodinov, and M. E. Kostanovskaya, “The thermal conductivity and emissivity of DE-24 graphite at temperatures of 23003000 K,” *Measurement Techniques*, vol. 53, no. 12, pp. 1380–1388, 2011.
- [24] B. Cockeram, D. Measures, and A. Mueller, “The development and testing of emissivity enhancement coatings for themophotovoltaic (TPV) radiator applications,” *Thin Solid Films*, vol. 355356, pp. 17–25, Nov. 1999.
- [25] R. K. Endo, Y. Fujihara, and M. Susa, “Calculation of the density and heat capacity of silicon by molecular dynamics simulation,” *High Temp High Press*, vol. 35, no. 36, pp. 505–511, 2003.
- [26] S. C. Wood, P. P. Apte, T.-J. King, M. M. Moslehi, and K. C. Saraswat, “Pyrometer modeling for rapid thermal processing,” pp. 337–348, 1991.
- [27] C. Liebert and R. Thomas, “Spectral Emissivity of Highly Doped Silicon,” Technical Note NASA TN D-4303, National Aeronautics and Space Administration, Washington D.C., 1968.

- [28] M. A. Green, “Self-consistent optical parameters of intrinsic silicon at 300K including temperature coefficients,” *Solar Energy Materials and Solar Cells*, vol. 92, pp. 1305–1310, Nov. 2008.
- [29] R. Santbergen and R. J. C. van Zolingen, “The absorption factor of crystalline silicon PV cells: A numerical and experimental study,” *Solar Energy Materials and Solar Cells*, vol. 92, pp. 432–444, July 2007.
- [30] Abderrahmane Belghachi, “Theoretical Calculation of the Efficiency Limit for Solar Cells Y1 - 2015-10-22 N1 47490 UR,” in *Solar Cells - New Approaches and Reviews*.
- [31] A. B. Sproul and M. A. Green, “Improved value for the silicon intrinsic carrier concentration from 275 to 375 K,” *Journal of Applied Physics*, vol. 70, no. 2, pp. 846–854, 1991.
- [32] K. Misiakos and D. Tsamakis, “Accurate measurements of the silicon intrinsic carrier density from 78 to 340 K,” *Journal of Applied Physics*, vol. 74, no. 5, pp. 3293–3297, 1993.
- [33] M. Thirugnanasambandam, S. Iniyar, and R. Goic, “A review of solar thermal technologies,” *Renewable and Sustainable Energy Reviews*, vol. 14, pp. 312–322, Jan. 2010.
- [34] “Basic Relations of Radiation,” in *Intermediate Heat Transfer*, Dekker Mechanical Engineering, CRC Press, Jan. 2003.
- [35] S. D. Shapiro, “Carrier mobilities in silicon empirically related to doping and field,” *Proc IEEE*, 1967.
- [36] C. K. Ho, A. R. Mahoney, A. Ambrosini, M. Bencomo, A. Hall, and T. N. Lambert, “Characterization of Pyromark 2500 Paint for High-Temperature Solar Receivers,” *Journal of Solar Energy Engineering*, vol. 136, no. 1, pp. 014502–014502, 2013.
- [37] M. Taylor, “Concentrating Solar Power,” tech. rep., International Renewable Energy Agency, Bonn, Germany, 2012.
- [38] “Concentrating Solar Power,” Tech. Rep. NREL/FS-550-48658, National Renewable Energy Laboratory, 1617 Cole Boulevard, Golden, Colorado 80401, 2010.
- [39] T. H. DiStefano, G. D. Pettit, J. M. Woodall, and J. J. Cuomo, “Conformal antireflective coatings on a textured tungsten surface,” *Applied Physics Letters*, vol. 32, no. 10, pp. 676–678, 1978.
- [40] K. Montgomery, C. Heredia, and J. Woodall, “Design and modeling of a high efficiency hybrid photovoltaic-photothermal concentrator (PVPTC) system,” in *Photovoltaic Specialists Conference (PVSC), 2013 IEEE 39th*, pp. 1755–1760, June 2013.

- [41] S. Picard, D. T. Burns, and P. Roger, “Determination of the specific heat capacity of a graphite sample using absolute and differential methods,” *Metrologia*, vol. 44, pp. 294–302, Oct. 2007. WOS:000250140500008.
- [42] “Electric Power Monthly,” independent Statistics & Analysis, U.S. Energy Information Administration, Oct. 2015.
- [43] “Electromagnetics and Electromagnetic Radiation,” in *Thermal and Flow Measurements*, pp. 351–366, CRC Press, Apr. 2008.
- [44] “Emissivity of Total Radiation for Various Materials,” in *CRC Handbook of Chemistry and Physics, 96th Edition (Internet Version 2016)* (W. Hanes, ed.), Boca Raton, FL: CRC Press/Taylor and Francis, 2016.
- [45] R. Brandt, C. Bird, and G. Neuer, “Emissivity reference paints for high temperature applications,” *Measurement*, vol. 41, pp. 731–736, Aug.
- [46] J. B. Chou, Y. X. Yeng, Y. E. Lee, A. Lenert, V. Rinnerbauer, I. Celanovic, M. Soljai, N. X. Fang, E. N. Wang, and S.-G. Kim, “Enabling Ideal Selective Solar Absorption with 2d Metallic Dielectric Photonic Crystals,” *Advanced Materials*, pp. n/a–n/a, 2014.
- [47] J. M. Woodall, “Energy Conversion,” Feb. 1982.
- [48] “Global Status Report 2014,” *Renewable Energy Policy Network for the 21st Century, Paris, France*, 2014.
- [49] W. Spitzer and H. Y. Fan, “Infrared Absorption in n-Type Silicon,” *Physical Review*, vol. 108, pp. 268–271, Oct. 1957.
- [50] P. P. R. Appl, “Modelling free-carrier absorption in solar cells,” *Progress in Photovoltaics: Research and Applications*, vol. 5, pp. 229–236, 1997.
- [51] M. A. Green and M. J. Keevers, “Optical properties of intrinsic silicon at 300 K,” *Progress in Photovoltaics: Research and Applications*, vol. 3, no. 3, pp. 189–192, 1995.
- [52] “Radiation Cooling,” in *Practical Guide to the Packaging of Electronics, Second Edition*, Dekker Mechanical Engineering, pp. 39–51, CRC Press, Dec. 2008.
- [53] Z. Zhang and D. P. DeWitt, “Radiation Heat Transfer,” in *Albright’s Chemical Engineering Handbook*, pp. 567–589, CRC Press, Nov. 2008.
- [54] G. B. Haxel, S. Boore, and S. Mayfield, “Rare Earth ElementsCritical Resources for High Technology,” Fact Sheet 087-02, U.S. Geological Survey, May 2005.
- [55] H. Wuester, R. Ferroukhi, L. El-Katiri, D. Saygin, T. Rinke, and D. Nagpal, “RE-thinking Energy: Renewable Energy and Climate Change,” tech. rep., International Renewable Energy Agency, 2015.

- [56] W. R. Runyan, *Silicon semiconductor technology*. New York: McGraw-Hill, 1965.
- [57] M. Wasfi, “Solar Energy and Photovoltaic Systems,” 2011.
- [58] M. Dunlap, W. Marion, and S. Wilcox, “Solar Radiation Data Manual for Flat-Plate and Concentrating Collectors,” Technical Report NREL/TP-463-5607 ON: DE93018229; TRN: 94:007521, National Renewable Energy Lab., Golden, CO (United States).
- [59] H. O. McMahon, “Thermal Radiation from Partially Transparent Reflecting Bodies,” *Journal of the Optical Society of America*, vol. 40, pp. 376–378, June 1950.
- [60] M. Planck, *The Theory of Heat Radiation*. QC: Science: Physics, P. Blakiston’s son & co., 1914.
- [61] D. Kearney, “Utility-Scale Power Tower Solar Systems: Performance Acceptance Test Guidelines,” Tech. Rep. NREL/SR-5500-57272, National Renewable Energy Laboratory, Golden, Colorado, Mar. 2013.
- [62] A. Luque, “Will we exceed 50% efficiency in photovoltaics?,” *Journal of Applied Physics*, vol. 110, Aug. 2011.